Geomorphology 472 (2025) 109583

Contents lists available at ScienceDirect

Geomorphology

journal homepage: www.journals.elsevier.com/geomorphology

Fault geometry, strain partitioning and deformation history inferred by fluvial topography and marine terraces analyses

F. Pavano *

Department of Earth Sciences, Environment and Resources, University of Naples Federico II, Via Vicinale Cupa Cintia 21, 80126 Naples, Italy

ARTICLE INFO

Keywords:
NE Sicily
River Long Profile Inversion
Marine Terraces
Tectonics

ABSTRACT

Advancements in the quantitative investigation of fluvial topography in tectonically active regions account for the emerging numerical modelling of river profiles and their linear inversions. Applications of a geomorphic approach strive for the reconstruction of long-term tectonic deformation histories by decoding base-level fall signals transiently embedded in the geomorphic record. I present integrated results from river profile inversions and marine terraces analyses, here used to outline the deformation model associated to a debated crustal fault system at the southern termination of the Calabrian Forearc High (Central Mediterranean). The study aims at constraining spatial and temporal variations in geometry, strain partitioning, slip rate, and time-transgressive propagation of the tectonic deformation associated with a fault system. In particular, I systematically analyze river profiles draining the eastern flank of the Peloritani Mts. in northeastern Sicily (southern Italy), a NNE-SSW-trending mountain ridge thought as located at the footwall of an active, ESE-dipping normal fault. I perform the linear inversions of fluvial topography by applying recently available MATLAB scripts, and I carry out the analysis of terraced surfaces by both GIS tools and MATLAB-based software packages. The results I obtain suggest that the eastern flank of the Peloritani Mts. have been deformed according to at least three main stages of uplift accommodated along distinct, ~10–15 km-long *en-échelon* arranged fault segments. The reconstructed evolution of tectonic deformation unveils time-transgressive, southward propagation since the last ~600 kyr, inset in a general increase, through time, of the regional component of uplift. The results of this study contribute to address the issues of the deformation style and strain partitioning along complex and/or debated fault systems. These results also demonstrate the potential of the geomorphic approach in defining the spatial and temporal tectonic evolutionary model of a region.

1. Introduction

Tectonically active regions experience relative base level changes due to the combination of tectonic uplift and climate-driven eustatic oscillations. Repeated base level falls (BLF) result in the emersion of marine erosional and depositional forms along the coast (e.g., marine terraces, shoreline angles, paleo-sea cliffs), and in the coeval upstream propagation of erosional waves (e.g., knickpoints). With the support of available high-resolution topographic data, these remnants of paleo-sea levels, worldwide well preserved when younger than MIS 11 (e.g., Saillard et al., 2011; Matsu'ura et al., 2019; Crosetto et al., 2024), together with transient fluvial landscape are classically employed to detect recent to active tectonic deformation, and relative rates, at both regional and local scales (e.g., Lajoie, 1986; Bloom and Yonekura, 1985; Kelsey and Bockheim, 1994; Catalano and De Guidi, 2003; Antonioli et al., 2006; Ferranti et al., 2010; Bowles and Cowgill, 2012; Yildirim et al., 2013; Jara-Muñoz et al., 2015, 2016, 2017; Pavano et al., 2016; Racano et al., 2020; Pavano and Gallen, 2021). However, many studies lack a detailed modelling of the fault system's geometry and fault segments arrangement, as well as their kinematic evolution and strain partitioning history. This is particularly true for coast-controlling faults, located offshore, being difficult any attempt of defining the kinematic evolution by direct observations and gauges along the structures. In general, all of these aspects have important repercussions on fault interactions models and on the definition of the seismic potential of a fault system.

The study area of the present work is one of the seismically most active regions in the Italian peninsula (Falcone et al., 2020; Rovida et al., 2022). It is located along the eastern Peloritani Mts. (NE Sicily, Italy), at the southern termination of the Calabrian Forearc. This latter is

* Corresponding author.
E-mail address: francesco.pavano@unina.it.

https://doi.org/10.1016/j.geomorph.2024.109583
Received 8 September 2024; Received in revised form 16 December 2024; Accepted 17 December 2024
Available online 24 December 2024

experiencing crustal fragmentation processes since the Middle-Late Pleistocene (Billi et al., 2010; Pavano et al., 2015, 2018; Totaro et al., 2016; Cammarata et al., 2018; Foti et al., 2023). The relief of the eastern side of the Peloritani Mts. is thought as controlled by an offshore normal fault (Taormina fault) (Catalano et al., 2008; Pavano et al., 2018), still debated (DISS Working Group, 2021) and belonging to a regional-scale extensional belt (Monaco and Tortorici, 2000; Catalano et al., 2008). Previous studies inferred the existence of the Taormina fault and its late Quaternary activity by integrated modelling of deformed geomorpho-stratigraphic markers (e.g., marine terraces, coastal notches, fluvial-deltaic deposits) along the coastal belt (Catalano and De Guidi, 2003; Catalano et al., 2003; De Guidi et al., 2002, 2003; Catalano et al., 2008; Spampinato et al., 2012; Aloisi et al., 2013; Pavano et al., 2016; Ferranti et al., 2017; Meschis et al., 2022; Pavano et al., 2024) and through the topography and fluvial networks (Goswami et al., 2012; Pavano et al., 2016, 2024; Meschis et al., 2019; He et al., 2021a). However, there is no data which could infer the detailed timing of fault activation and the spatio-temporal distribution of deformation.

The goal of the present work is, thus, to detail the base level fall history along the eastern Peloritani Mts. ridge, to portray the geometrical and kinematics character of the bounding fault, and to understand the propagation timing of long-term, fault-related uplift signal through the studied region. More widely, the paper wants also to enlarge the field of application of the river longitudinal profiles inversion analysis, contributing in bridging the age resolution gap between those resulting from the analysis of the paleo-sea level markers along the coast (e.g., marine terraces, paleo-shorelines) (10^3–10^5 yrs) and the longer-time ones obtained by applying classical geological approach (10^6 yrs).

Specifically, I combine the inversion of fluvial topography with the analysis of marine geomorphic markers, in order to explore if and how the watersheds differentially have recorded variable, both in time and space, tectonic signals.

The obtained results allow to extend back to the entire middle Pleistocene the age model inferred by marine terraces and fluvial topography analyses, detailing the evolutionary stages and the pattern of deformation at both local and regional scale.

2. Geological and tectonic settings of the study area

The Peloritani Mts., in northeastern Sicily (southern Italy), are located at the southern end of the SE-ward translating Calabrian Forearc (Amodio-Morelli et al., 1976; Scandone, 1979; Lentini et al., 1996; Rosenbaum and Lister, 2004; Faccenna et al., 2011) (Fig. 1A). In the framework of the Ionian subduction system, the Calabrian Forearc High represents a backstop, located between the NW-ward subducting Ionian oceanic crust slab, to the SE front, and the recently opening of the ocean-like Tyrrhenian basin, at the rear (Amodio-Morelli et al., 1976; Malinverno and Ryan, 1986; Dewey et al., 1989; Boccaletti et al., 1990; Lentini et al., 1995; Malinverno, 2012; Faccenna et al., 2014). The geological backbone of the Calabrian orocline results from several tectono-metamorphic units (Cirrincione and Pezzino, 1994; Olivetti et al., 2010; Catalano et al., 2018) piled up during the Eocene, and organized with the high-grade metamorphic terranes at the top of the stack, and the low-grade metamorphic units occupying the lowest position (Lentini and Vezzani, 1975; Lentini et al., 2000). The Peloritani Ridge (Fig. 1B) is surrounded by Miocene to Pleistocene clastic terrains mostly hosted within fault-controlled depositional environments (Catalano and Cinque, 1995; Lentini et al., 1995; Lentini et al., 2000; Pavano et al., 2024; Di Stefano and Longhitano, 2009) (Fig. 1B).

Since the middle Pleistocene, the dynamics of the Calabrian Forearc High is dominated by regional-scale extension (Monaco and Tortorici, 2000; Catalano et al., 2008) (see inset in Fig. 1), accommodated along discrete fault segments with length in the order of 10^1 km. This extensional belt deforms the western side of Calabria, from the Serre Massif to the Messina Strait, and controls the entire coastal belt of eastern Sicily, from the Peloritani Mts. up to the reactivated Malta Escarpment, passing through the eastern flank of Mt. Etna Volcano (*E* in the inset of Fig. 1) (Monaco et al., 1995, 2005; Bianca et al., 1999; Monaco et al., 2002; Argnani and Bonazzi, 2005; Catalano et al., 2010). In particular, the southern termination of the Calabrian Forearc High is experiencing middle-late Pleistocene crustal fragmentation (Fig. 1B) (Billi et al., 2010; Pavano et al., 2012, 2015; Catalano et al., 2012; Cammarata et al., 2018), consequent to its eastward transit along the northern belt of Sicily (Pavano and Gallen, 2021). This fragmentation is currently accommodated by a dominant negative inversion of pre-existing, multi-

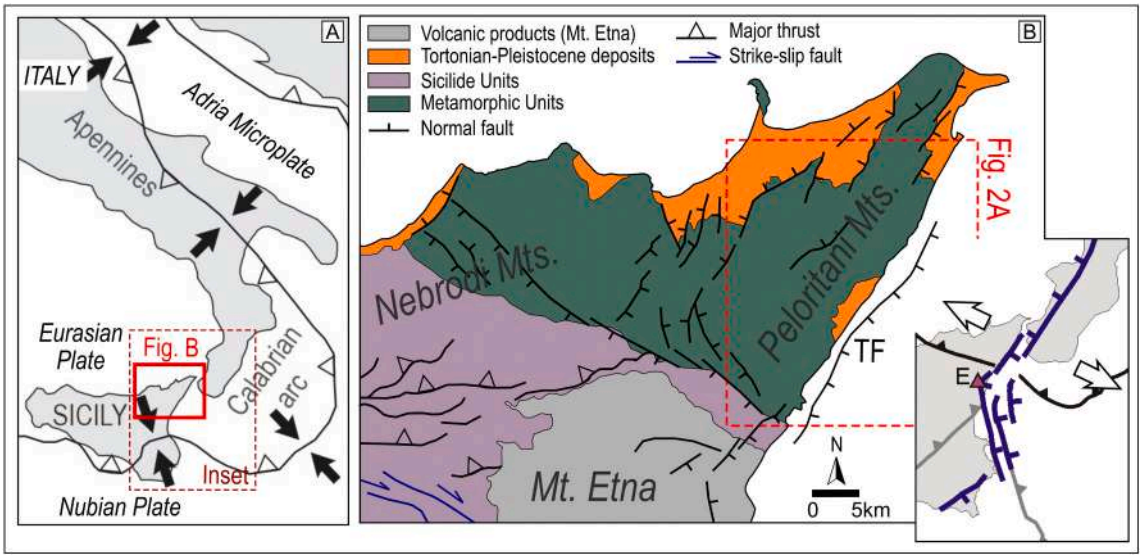

Fig. 1. A) Sketch map of the geodynamic framework of the central Mediterranean, focused on the central-southern portion of the Italian peninsula, along the Nubia-Eurasia convergent plate boundary. B) Schematic geological-structural map of northeastern Sicily, showing the distribution of the rock units and the principal fault systems. The inset map shows the regional-scale extensional belt controlling both eastern Sicily and western Calabria (Monaco and Tortorici, 2000; Catalano et al., 2008) (mod. from Pavano and Gallen, 2021). E: Mt. Etna; the black and the grey lines with triangles refer to the front of the European crystalline units and to the front of the Apenninic-Maghrebian allochthonous units, respectively; the blue lines with ticks represent normal faults. The two arrows indicate the extension affecting the NE-Sicily region.

stages fault systems (Ghisetti, 1979; Lentini et al., 1995, 1996; Pavano, 2013; Pavano et al., 2015, 2018; Foti et al., 2023).

The eastern coast of the Peloritani Mountains is located at the footwall of a NNE-SSW-oriented branch of this regional scale extensional belt, the Taormina Fault (*TF* in Fig. 1B) (Catalano et al., 2008; Catalano and De Guidi, 2003). This ~30 km-long ESE-dipping fault is debatably supposed to control the uplift of the Peloritani ridge, being located at its near offshore (Catalano et al., 2008; De Guidi et al., 2002, 2003). This latter aspect implied uncertainties in determining the actual geometry of the fault, the arrangement and the activity timing of the composing fault segments (De Guidi et al., 2002; Argnani et al., 2009; Barreca et al., 2019), as well as difficulties in defining the seismic potential of this structure and the association with paleo-earthquakes (Catalano et al., 2003; De Guidi et al., 2003; Azzaro et al., 2007; Meschis et al., 2022). The late Quaternary activity of the Taormina Fault has been drawn through geomorphic evidences inland, such as topographic data, uplifted remnants of marine terraces and notches (Stewart et al., 1997; Rust and Kershaw, 2000; Catalano and De Guidi, 2003; Ferranti et al., 2017; Meschis et al., 2019), and base-level-fall-related upstream-migrating knickpoints (Pavano et al., 2016). Recently, multiapproach stratigraphic and geomorphic studies tried to unravel long-term tectonic evolution of the Messina Strait area, net of the contribution from eustatic changes and sedimentary accommodation space variation (Dorsey et al., 2023; Pavano et al., 2024).

3. Methods

All of the geomorphic analyses performed in the present study are based on querying a LiDAR data-derived Digital Elevation Model (DEM) with a resolution of 2 m (source: Sicily Region – Territory and Environment Department). I used this DEM to extract the drainage network of 12 main catchments draining the eastern flank of the Peloritani Mountains (Fig. 2). I set a threshold for the upslope area of 0.25 km^2, less than the commonly used 1 km^2 (Montgomery and Foufoula-Georgiou, 1993; Wobus et al., 2006), and chosen on the basis of the small size of the analyzed drainage basins (~6 to ~80 km^2; average = ~23 km^2) and their relatively steep headwaters.

3.1. River profile analysis

The performed longitudinal river profile (hereafter river profile) analysis has its foundation into the stream power incision rule, represented by a power function that relates long-term bedrock channel erosion (E; m yr^{-1}) to the drainage area (A; m^2) (a proxy of drainage discharge) and the channel slope (S), scaled by the erodibility constant (K; $m^{0.1}$ yr^{-1}):

$$E = KA^m S^n \quad (1)$$

where m and n are dimensionless exponents (Whipple and Tucker, 1999; Whipple et al., 2000). For the case of detachment-limited plucking erosion process (Hancock et al., 1998), previous studies (e.g., Whipple et al., 2000) have shown that n = ~1, allowing simplifications in applying the stream power incision rule equations (see Supplementary Information SI1). Although some studies found $n > 1$ (e.g., DiBiase et al., 2010; Lague, 2014; Harel et al., 2016; Gallen and Fernández-Blanco, 2021), which would account for different erosional mechanisms, the assumption of $n = 1$ would be here corroborated by the linear relationship between long-term incision rates and k_{sn} found for the study area by previous works (Pavano et al., 2016). However, in general, I acknowledge that $n = 1$ is still an assumption and that n could actually have varied through time and spatially through the fluvial network, especially due to variation in erosion rates and sediment fluxes (e.g., due to fluvial knickpoints' migration, climate-driven K modulation).

In order to carry out the river profile modelling I follow the integral approach proposed by Perron and Royden (2013). This approach accounts for the elevation integral (χ, *Chi*) of a river profile (i.e. χ-transformed profile) as a prediction of the steady state elevation of a channel, and also applied for exploring drainage divide's reorganization dynamics in combination with some Gilbert metrics (Willett et al., 2014; Forte and Whipple, 2018). Specifically, χ represents the equation of a line in a χ-elevation space (χ-plots) (i.e. when $A_0 = 1$ and $n = 1$; Smith et al., 2022), with k_{sn}, which is the steepness index normalized by using a reference concavity (Whipple and Tucker, 1999; Snyder et al., 2000; Whipple, 2004; Wobus et al., 2006; Gailleton et al., 2021), representing the line's slope (Perron and Royden, 2013) (see Supporting Information SI1). A concavity reference value of 0.45 is widely applied in river profiles analyses and it is here chosen as reference firstly based on previous works (Pavano et al., 2016). Beyond the value of $\theta = 0.5$ found at global scale (Harel et al., 2016), in many regions through the Italian peninsula several authors found average θ values ranging between 0.40 and 0.45 (Olivetti et al., 2012; Fisher et al., 2022; Gallen et al., 2023; Clementucci et al., 2024), with some exceptions in some areas of the NW and Central Apennines (Buleo Tebar et al., 2024; Racano et al., 2024). Particularly for NE-Sicily, and specifically for the study area, Pavano et al. (2016) calculated an average θ value of 0.44 for the drainage basins draining the eastern flank of the Peloritani Mts. Here, I also carried out a best θ (i.e. m/n ratio) search analyses (Fig. S1 in SI1), which provided a value of ~0.43, further justifying the choice of 0.45 as reference concavity.

To extract channels from the drainage network and to model them in χ-Elevation space I use the MATLAB-based TopoToolbox and TAK software packages (Schwanghart and Scherler, 2014, 2017; Forte and Whipple, 2019). In particular, I perform the linear inversion modelling of the χ-transformed river profiles by running available MATLAB-written scripts (Gallen, 2018), earlier modified and applied in Sicily (Pavano and Gallen, 2021) and recently optimized and used in the Apennines (Fisher et al., 2022; Pazzaglia and Fisher, 2022) (https://zenodo.org/record/6503006#.Y8FY0tLMI9F), based on the "Block Uplift" model of Goren et al. (2014).

In order to calculate the rock-dependent erodibility coefficient (K) (see Eq. 4 in SI1) for each outcropping rock type, I used the value E = ~1.0 mm/yr, provided in the literature from basin-integrated ^{10}Be-based erosion rate (Cyr et al., 2010; Pavano et al., 2024), and the χ-discretized k_{sn}. I iterated 2000 times the code (Fisher et al., 2022) by using a Monte Carlo routine, run varying simultaneously E and k_{sn} in order to propagate the uncertainties of these two parameters and of K within the calculation of the fluvial system's response time and, thus, within the reconstruction of the base level fall histories.

Following the "Block Uplift" method (Goren et al., 2014), and assuming $n = 1$, once determined K for χ-binned k_{sn} values, I invert for base-level fall history, by converting a non-dimensional base level fall (Goren et al., 2014) to rock-uplift via χ profile inversion, and do a dimensional inversion of the tau plot. A more detailed explanation of the theoretical basis and applications of the linear inversion approach, and a deeper understanding of the applied method is provided in the Supplementary Information 1 and 2 (SI1 and SI2), as well as in several recent publications (Goren et al., 2014; Gallen, 2018; Pavano and Gallen, 2021; Fisher et al., 2022; Pazzaglia and Fisher, 2022).

Given that the drainage systems of the eastern flank of the Peloritani Mts. has been demonstrated to be sensitive to the eustatic fluctuations of the sea level (Pavano et al., 2016, 2024), in order to obscure or minimize the signals of eustasy in the reconstructed base level fall histories I set the time (τ) discretization of the block uplift model with increments of 0.05 Myrs. This time frame, which corresponds to increments in χ ranging in value between 760 and 1300, matches the sensitivity test results, showing low misfit when using >6 increments to discretize χ space (Fig. S3 in SI3).

The inverted river profiles have the current shoreline as base level, although a very narrow coastal plain characterize the coastal belt of the study area and alluvial deposits occupy the final sector of the outlet of the analyzed channels. As recently demonstrated, the base level fall

history reconstructed by river profile inversion does not change even excluding from the experiments the present-day alluviated (Pavano et al., 2024; Peloritani Mts.) or recently emerged (Racano et al., 2023; Pontide Mountains) short coastal belt.

Then, the base level fall rate history data interpretation carries on by selecting those peaks that emerge from a ~1.0 mm/yr background signal, a rate proposed as a long-term regional signal of uplift by several independent studies (e.g., Catalano and Di Stefano, 1997; Ferranti et al., 2006; Catalano et al., 2008; Pavano et al., 2015, 2016; Meschis et al., 2018; Pavano et al., 2024). Secondly, I filtered the data for amplitudes higher than 0.2 mm/yr, which is a reasonable threshold lying beyond the average errors associated with the modelled rate values.

3.2. Marine terraces modelling

The marine terraces analysis accounts for two main approaches, performed by using the MAP and the LEM modules available in the MATLAB-based software package TerraceM-2 (Jara-Muñoz et al., 2019), which allowed to map and model the marine terraces' distribution.

I approach: I firstly both manually and (semi-)automatically model the elevations' distribution of the marine terraced surfaces and shoreline angles correlative to sea-level highstands (Weber, 1990), and recognized along 20 sections selected along the coast (Fig. 2A). This stage of analysis benefited the support of geomorphological field surveys and observations. In this analysis, I further manually exclude the terraced surfaces with fluvial origin, according to a few efficient criteria, such as their location along, and parallel to active (or hanging) (paleo-)channels, or their elongated and narrow shape confined between two topographic ridges. For the I approach, I use the MAP module to perform both manual (Shoreline angle mapping tool) and semi-automatic (Surface Classification Model - SCM mapping tool; Bowles and Cowgill, 2012) detection of terraced surfaces. I used these two tools as complementary of each other. For the SCM tool, in order to isolate flat and smoothed patches of landscape from the steep and vertically-incised ones, I used cutoff values of slope and topographic roughness of ~15–20° and ~1.5–2.0, respectively (Bowles and Cowgill, 2012) (Fig. 2B). I also used elevation ranges of ~15–25 m (Fig. 2C and SI6) to differentiate distinct terraces' levels (Fig. 2D), later checked by field-

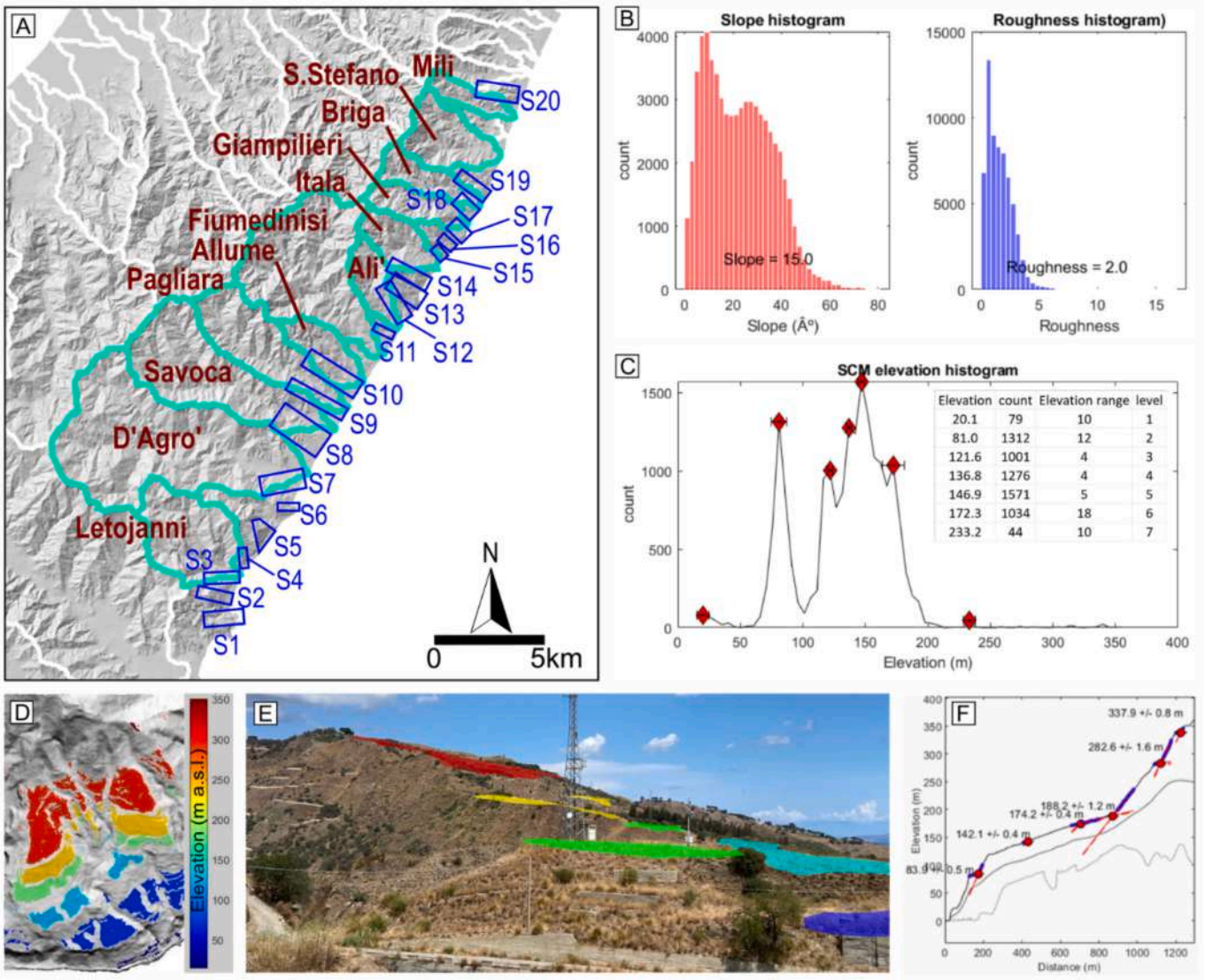

Fig. 2. A) Map showing the analyzed drainage basins and the sections selected for marine terraces and paleo-shoreline angles analyses, along the eastern flank of the Peloritani Mts. B) geomorphic parameters (topographic slope and roughness) used to isolate flat and smoothed patches of landscape. C) Elevation histogram of the detected levels of marine terraces, showed together with the related data table. D) Example (section 17) of terraced surfaces mapped by SCM tool. E) Field observation of the terraced surfaces showed in D). F) steps-like section (section 17) showing terraced surfaces recognized by the shoreline angle mapping tool in MAP module of TerraceM-2 software.

based geomorphological survey (Fig. 2E). In addition, by the shoreline angle mapping tool I recognize staircase-like landforms by a supervised analysis along the selected 20 sections (Fig. 2F).

II approach: for selected sections, a second approach allowed to perform a modelled prediction of the marine terraces' distribution along the studied coastal belt. In order to do this, I combine the discretized rock uplift records reconstructed for the last 350 ka by river profiles inversions, together with the reference eustatic sea level changes for the last ~450 ka (Waelbroeck et al., 2002). As boundary conditions for the LEM setting, I use a coastal slope angle of 10°, which is the average value of costal slope at several locations along the study area, and a maximum wave height of 4 m, provided by the Copernicus Marine Service for the nearshore belt of the NE-Sicily, and estimated for a time range covering the last three years. As for the reference sea level changes curve, after a comparison between the most used in the literature for the Mediterranean area (Waelbroeck et al., 2002; Bintanja et al., 2005; Rohling et al., 2014), I selected the one proposed by Waelbroeck et al. (2002). In fact, using this latter one produces the lowest discrepancy between modelled and mapped marine terraces elevations (SI4). In addition, the Waelbroeck et al. (2002) sea level changes curve is in good agreement with the distribution of <MIS 9 speleothems sampled in the Mediterranean area (Antonioli et al., 2021).

For the II approach, I use the LEM module in TerraceM-2 software to predict the positions of marine terraces (Jara-Muñoz et al., 2017; Racano et al., 2020) in a framework of complex time-dependent variation in uplift rate. Since the marine terrace mainly consists of abrasion platforms, and secondarily, when marine deposits can be recognized, they are thin (1–1.5 m) (Antonioli et al., 2006; Meschis et al., 2022), I do not consider the base of these deposits as reference elevation for the modelling. The LEM approach accounts for the marine terraces' reoccupation (Merritts and Bull, 1989; Kelsey, 1990; Nalin et al., 2007; Melnick, 2016; Oakley et al., 2017; Malatesta et al., 2021; Crosetto et al., 2024) and their dependency on the time spent within the sea erosional depth (Trenhaile, 2019; Malatesta et al., 2022; Crosetto et al., 2024), as a combination of eustasy and rock uplift. In more detail, I considered variable uplift rate, both spatially and temporally, condensed in four main time steps: 350 ka, 250 ka, 150 ka, 0 ka. For these four time-steps, I use the corresponding BLF rates values.

Once obtained the data, I compared the flights of marine terraces resulting by these two independent approaches (Fig. 2E–F), thus exploring their matching and discrepancies in terms of both elevations and uplift rates.

I additionally used some available geochronological ages as independent constrains to build an age model for marine terraces and to calculate uplift rates. Specifically, I used the available IRSL ages of middle-late Pleistocene fluvio-deltaic deposits (Messina Gravel and Sands - MGS). In this regard, in the area of Pagliara basin (~ sections 9-to-11; Fig. 2), these deposits crop out at elevation up to 300–350 m a.s.l. (Pavano et al., 2024), and are approximately consistent with the paleo-shoreline location. As references, I also consider ESR-based (Electron Spin Resonance technique) ages available for MIS 5.5 marine terraces (Antonioli et al., 2006) located at elevation of 115 m a.s.l., in the area of section 1 (Fig. 2). Finally, I also crosschecked the resulting data with the marine terraces' age models proposed for the same area in previous works by different approaches (geomorphological and/or bio-stratigraphical) (Catalano and De Guidi, 2003; Antonioli et al., 2006; Ferranti et al., 2006, 2010; Pavano et al., 2016; Meschis et al., 2022).

4. Results

4.1. Base level fall histories from rivers profile analysis

The reconstructed base level fall (BLF) rate histories take the modelled rivers' topography back in time up to ~0.7–0.9 Ma (Fig. 3, Table 1, and SI5). In general, the reconstructed BLF rate histories show a two-component signal. A background increasing trend of the signal is several times interrupted by the occurrence of single peaks in BLF rate, which are characterized by variable amplitude and time duration. It is noteworthy that the average modelled base level fall rate of about 1.01 ± 0.10 mm/yr (Table 1) is not so much different than the regional tectonic uplift rate estimations (1.1 mm/yr) available for this side of the NE Sicily (Catalano and De Guidi, 2003; De Guidi et al., 2003; Catalano et al., 2008; Pavano et al., 2016; Meschis et al., 2022; Pavano et al., 2024). Thus, a long-term increment in base level fall rate (potentially regional uplift) is inset by relatively higher-frequency peaks. These signals cannot be associated with an eustatic input, being this latter almost filtered (or dampened) by setting a τ intervals of 50 kyr (see Section 3.1).

By accounting for the spatial and time occurrence of those spikes in BLF rate over the ~1.0 mm/yr background signal (see Section 3) (Table 2), it emerges that they are time-transgressively distributed along the study area. In particular, I find that the BLF rate histories, net of the background uplift contribution, can be roughly discretized into three different evolutionary time stages (0–250 ka; 250–500 ka; >500 ka) and within three different sectors along the coast: the northern sector (Mili and S. Stefano basins), the central sector (from Briga to Ali' basins), and the southern sector (from Fiumedinisi to Letojanni basins). In particular, the BLF rate records modelled for the norther catchments (e.g., Mili, S. Stefano basins) (Fig. 3A and F and Fig. 4A) recorded the oldest (~0.5 Ma) occurrence of fast base level falls. Proceeding towards the south, in correspondence of the central portion of the study area (e.g., Giampilieri, Ali', Fiumedinisi basins) (Fig. 3B–C and G–H and Fig. 4B), most of the inverted catchments provide a BLF rate history showing the presence of two main peaks, one crudely older than ~0.4–0.5 Ma and one roughly younger than ~0.25–0.3 Ma. Finally, the southernmost catchments (e.g., Savoca, Letojanni basins) (Fig. 3D–E and I–J and Fig. 4C) show essentially only one dominant BLF rate peak, generally younger than ~0.3 Ma.

A complete pattern of the time and space distribution of the BLF rate record is displayed in Table 1, where the detailed variations in BLF rate for each catchment and for each discretized 50kyr-long time interval are showed by a warming color palette. Moreover, by accounting for rates variations ≥0.2 mm/yr, the southward younging of the local onset of fast base level fall rates becomes clearer (Table 2).

The general half-elliptical trend of the whole base level fall rate records, mimicking the deformation pattern modelled for a normal fault's footwall (e.g., Scholz and Gupta, 2000; Gupta and Scholz, 2000; Nicol et al., 2010), shows a gentle bimodal spatial distribution, with a wave length of ~15 km, if averaged and plotted against distance along the coast (Table 1 and Fig. 4D), and an almost uniformly increasing trend, when averaged and plotted against time (Table 1 and Fig. 5).

4.2. Marine terraces and paleo-shorelines analyses

By using the SCM tool in the MAP module of TerraceM-2 software, within the 20 investigated sections I found up to 13 levels of terraced surfaces (Table 3 and Fig. S6-1 in Supplementary Information SI6) (ordered with roman numbers from the highest terrace downward). These latter are almost homogeneously distributed along the entire studied belt, except for the most elevated and oldest orders (e.g., horizons I to III), which mostly lie at sections 2, 13 and 14 (Fig. 6A). Geometrically, the distribution of the terraces' levels draws a general convex-upward shape, in good agreement with previous data (e.g., Catalano and De Guidi, 2003). Specifically, excluding the I and II orders, which show very few data, I distinguished at least three main time-dependent different distribution patterns of terraces.

The first terraces distribution pattern (hereafter **tdp_1**), affecting old terraces from the I to the VI order and associated with ages ranging between 570 ka (MIS 15) and 305 ka (MIS 9), refers to an asymmetric, northward skewed, trend. The maximum in elevations is reached in the area of the Ali' basin, which generally gently reduces towards the south (Fig. 6A). Actually, the hinge zone of the drawn antiformal geometry

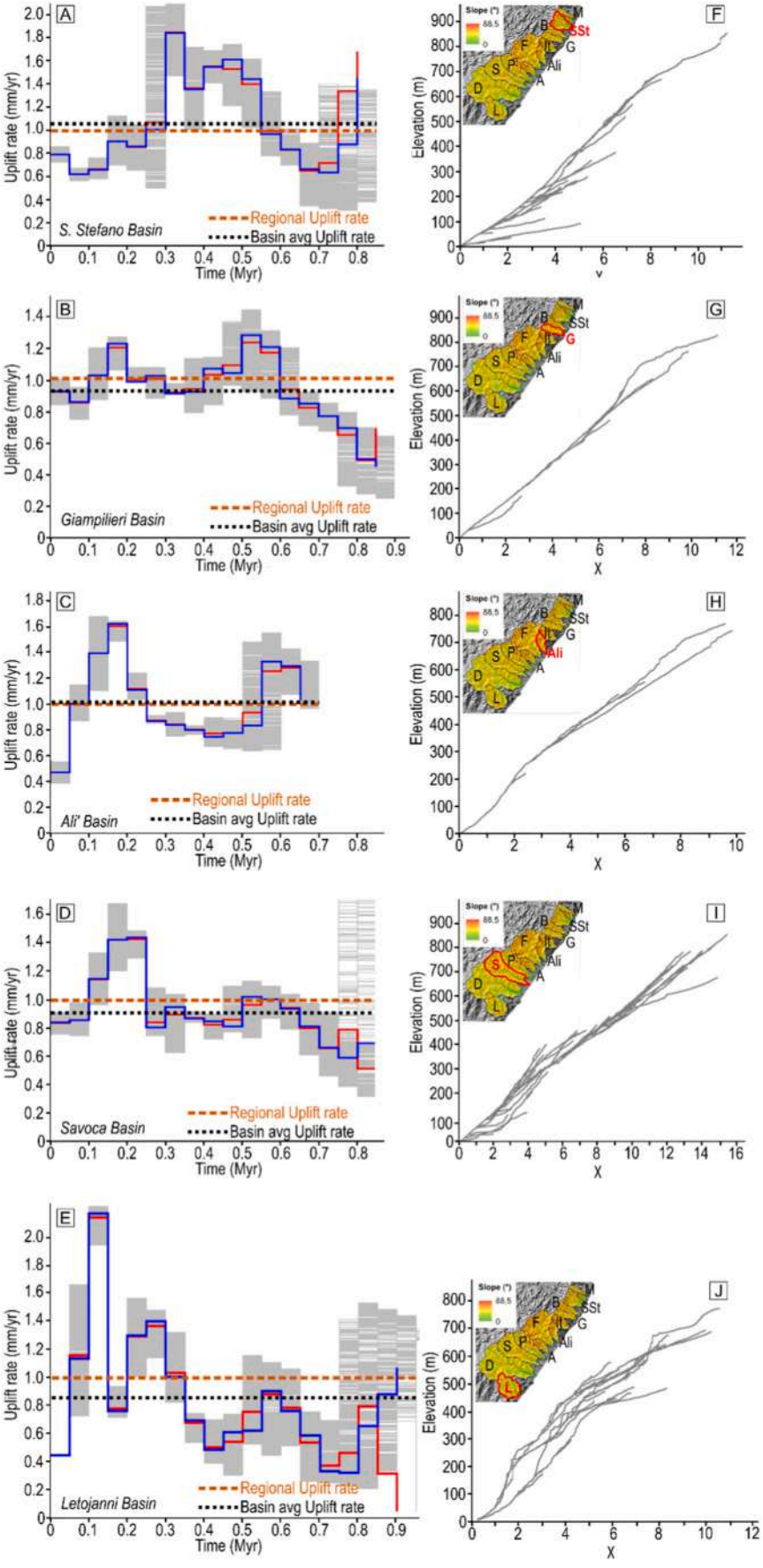

(caption on next page)

Fig. 3. A–E) U-τ plots derived by river profile inversions analysis. The red and the blue curves represent the averaged and the median U, respectively. The plot shows also the references regional uplift rate (orange dashed line) and the basin-averaged uplift rate (dashed black line). The shaded area derives from the overlapping of 2000 Monte Carlo iterations of river profile inversion. F–J) Corresponding χ-plots. L: Letojanni basin; D: Dagro' b.; S: Savoca b.; P: Pagliara b.; A: Allume b.; F: Fiumedinisi b.; Ali: Ali' b.; It: Itala b.; G: Giampilieri b.; B: Briga b.; SSt: S. Stefano b.; M: Mili b.

Table 1
Uplift rate values for the different catchments draining the eastern flank of the Peloritani Mts. obtained by inverting their fluvial topography. The grey-to-red colors palette displays the low-to-high rates. The last row shows the uplift rate values averaged for each 50 kyrs time interval. The column to the right shows the uplift rate values averaged for each of the analyzed catchments.

Age (ka) ->	*0*	*50*	*100*	*150*	*200*	*250*	*300*	*350*	*400*	*450*	*500*	*550*	*600*	*650*	*700*	*750*	*800*	*850*	*900*	*950*	*1000*	*Avg U*
Mili	0.66	0.8	0.67	0.95	0.97	**1.49**	**1.75**	**1.18**	**1.01**	0.94	**1.03**	**1.18**	**1.42**	**1.5**								1.11
Sstefano	0.79	0.62	0.66	0.9	0.86	1	**1.84**	**1.35**	**1.55**	**1.61**	**1.44**	0.97	0.83	0.66	0.62	0.88	**1.45**					1.08
Briga	0.78	0.82	**1.13**	**1.12**	**1.14**	0.92	**1.2**	**1.21**	0.89	0.92	0.96	0.88	0.81	0.83	0.97	0.78						0.97
Giampilieri	0.93	0.86	**1.03**	**1.23**	0.99	**1.02**	0.91	0.92	**1.07**	**1.04**	**1.28**	**1.21**	0.88	0.85	0.77	0.7	0.5	0.45				1.02
Itala	0.86	0.89	0.95	**1.06**	1	**1.1**	**1.13**	**1.24**	**1.22**	0.94	0.87	**1.06**	0.99	0.72	0.66	0.6	0.56	0.53				1.00
Ali	0.47	1	**1.39**	**1.62**	**1.11**	0.87	0.83	0.8	0.74	0.78	0.83	**1.33**	**1.29**	**1.03**								1.01
Fiumedinisi	0.8	0.74	0.95	**1.05**	**1.13**	**1.17**	**1.15**	**1.26**	**1.16**	0.95	0.99	0.78	0.73	0.86	0.95	**1.09**	0.93	0.75	0.42			0.98
Allume	0.83	0.66	0.97	**1.45**	0.97	**1.37**	0.88	0.85	0.87	0.98	**1.05**	0.98	**1.35**	**1.2**								1.03
Pagliara	**1.28**	0.94	0.8	0.71	0.81	0.98	**1.33**	**1.08**	**1.12**	**1.11**	1	0.99	**1.04**	0.93	0.87	0.84	0.76	0.65	0.48			1.01
Savoca	0.84	0.85	**1.15**	**1.42**	**1.44**	0.8	0.95	0.87	0.85	0.81	**1.01**	1	0.93	0.81	0.66	0.59	0.69					0.98
D'Agro'	0.83	0.77	0.71	0.68	**1.44**	**1.02**	**1.23**	**1.67**	**1.01**	**1.06**	0.91	0.82	0.86	0.97	0.95	0.91	0.88	0.36	0.32	0.35	0.94	1.00
Letojanni	0.45	**1.14**	**2.17**	0.76	**1.3**	**1.4**	1	0.69	0.49	0.61	0.62	0.9	0.76	0.58	0.33	0.32	0.65	0.88	**1.07**			0.92
Avg U	*0.79*	*0.84*	*1.05*	*1.08*	*1.1*	*1.1*	*1.18*	*1.09*	*1*	*0.98*	*1*	*1.01*	*0.99*	*0.91*	*0.75*	*0.75*	*0.8*	*0.6*	*0.57*	*0.35*	*0.94*	1.01

shifts slightly southward if accounted for youngest terraces (Fig. 6A). A bimodal distribution (hereafter **tdp_2**) mainly characterizes the marine terraces from the VII to the IX orders, which are associated with ages between 280 ka (MIS 8) and 200 ka (MIS 7). Marine terraces show two more or less marked bulges embedded within a general regional-scale antiformal geometry; specifically, one peak is located in the northern sector with its maximum roughly in correspondence of the Ali' basin area (approximately the same of **tdp_1**), and a second peak more to the south, reaching its elevations' maximum in the surroundings of D'Agro' basin area. This bimodal distribution does not markedly impact the older terraces, being reasonably masked or smoothed into half-elliptically already deformed horizons (Fig. 6A). Finally, the coast-parallel spatial distribution of the four youngest (X-to-XIII order) marine terraces levels (with ages <200 ka – <MIS 7) show a single convex-upward trend (hereafter **tdp_3**), almost centered in the area of the Pagliara basin (Fig. 6A).

The semiautomatic picking of paleo-shoreline angles (hereafter **psla**) along the same 20 sections (Fig. S6-2 in Supplementary Information SI6), provides results well matching the data from the SCM analysis, overall showing a similar antiformal trend. Differently than the SCM tool, the psla mapping results in the recognition of 18 paleo-sea level horizons, in good agreement with previous works (e.g., Meschis et al., 2022). These paleo-shoreline markers are dispersed in an elevation range between ~20 m and ~ 750 m above the current sea level and attributed to ages ranging between 40 ka and 570 ka.

Furthermore, some of the recognized psla can be barely outlined by very few data, recognized and laterally correlated along only few sections. This is the case of the most elevated levels (e.g., I-to-IV orders) (Fig. 6B), and of those well recognized along few sections at the southern half of the investigated coastal belt (e.g., X and XII levels) (Fig. 6B).

Similar to the SCM analysis, the mapped psla are organized in three stacked along-coast different distributions. The uppermost one, which involves the psla of the III-to-VI orders (and potentially also the I and II orders) and ranging in age between 570 ka and 330 ka (Fig. 6B), shows a northward skewed shape with the maximum elevations reached in correspondence of the Ali'-Itala basins' area, reproducing the tdp_1 of

Table 2
Uplift rate values (over the regional component of 1.0 mm/yr) for the different catchments draining the eastern flank of the Peloritani Mts. The values in bold refer to U ≥ 0.2 mm/yr. The light yellow-to-red colors palette displays the low-to-high rates. The data table is discretized into three different evolutionary time stages (0–250 ka; 250-500 ka; >500 ka) and three different sectors along the coast: the northern sector (Mili and S. Stefano basins), the central or transitional sector (Briga to Ali' basins), and the southern sector (Fiumedinisi to Letojanni basins). The table shows how uplift rates signals occurred time-transgressively from north to south and potentially along different fault segments, devoting attention to base level fall rate values higher than 0.2 mm/yr. The table also shows rate values averaged for both basins (column to the right) and ages (row at the bottom).

Age (ka) ->	*0*	*50*	*100*	*150*	*200*	*250*	*300*	*350*	*400*	*450*	*500*	*550*	*600*	*650*	*700*	*750*	*800*	*850*	*900*	*950*	*1000*	Avg U
Mili						**0.49**	**0.75**	0.18	0.01		0.03	0.18	**0.42**	**0.5**								0.32
Sstefano							**0.84**	**0.35**	**0.55**	**0.61**	**0.44**						**0.45**					0.54
Briga			0.13	0.12	0.14		**0.2**	**0.21**														0.16
Giampilieri			0.03	**0.23**		0.02			0.07	0.04	**0.28**	**0.21**										0.13
Itala				0.06		0.1	0.13	**0.24**	**0.22**			0.06										0.14
Ali			**0.39**	**0.62**	0.11							**0.33**	**0.29**	0.03								0.30
Fiumedinisi				0.05	0.13	0.17	0.15	**0.26**	0.16							0.09						0.14
Allume				**0.45**		**0.37**					0.05		**0.35**	**0.2**								0.28
Pagliara	**0.28**						**0.33**	0.08	0.12	0.11			0.04									0.16
Savoca			0.15	**0.42**	**0.44**						0.01											0.26
D'Agro'					**0.44**	0.02	**0.23**	**0.67**	0.01	0.06												0.24
Letojanni		0.14	**1.17**		**0.3**	**0.4**													0.07			0.42
Avg U	*0.28*	*0.14*	*0.37*	*0.28*	*0.26*	*0.22*	*0.38*	*0.28*	*0.16*	*0.21*	*0.16*	*0.2*	*0.28*	*0.24*		*0.09*	*0.45*		*0.07*			0.26

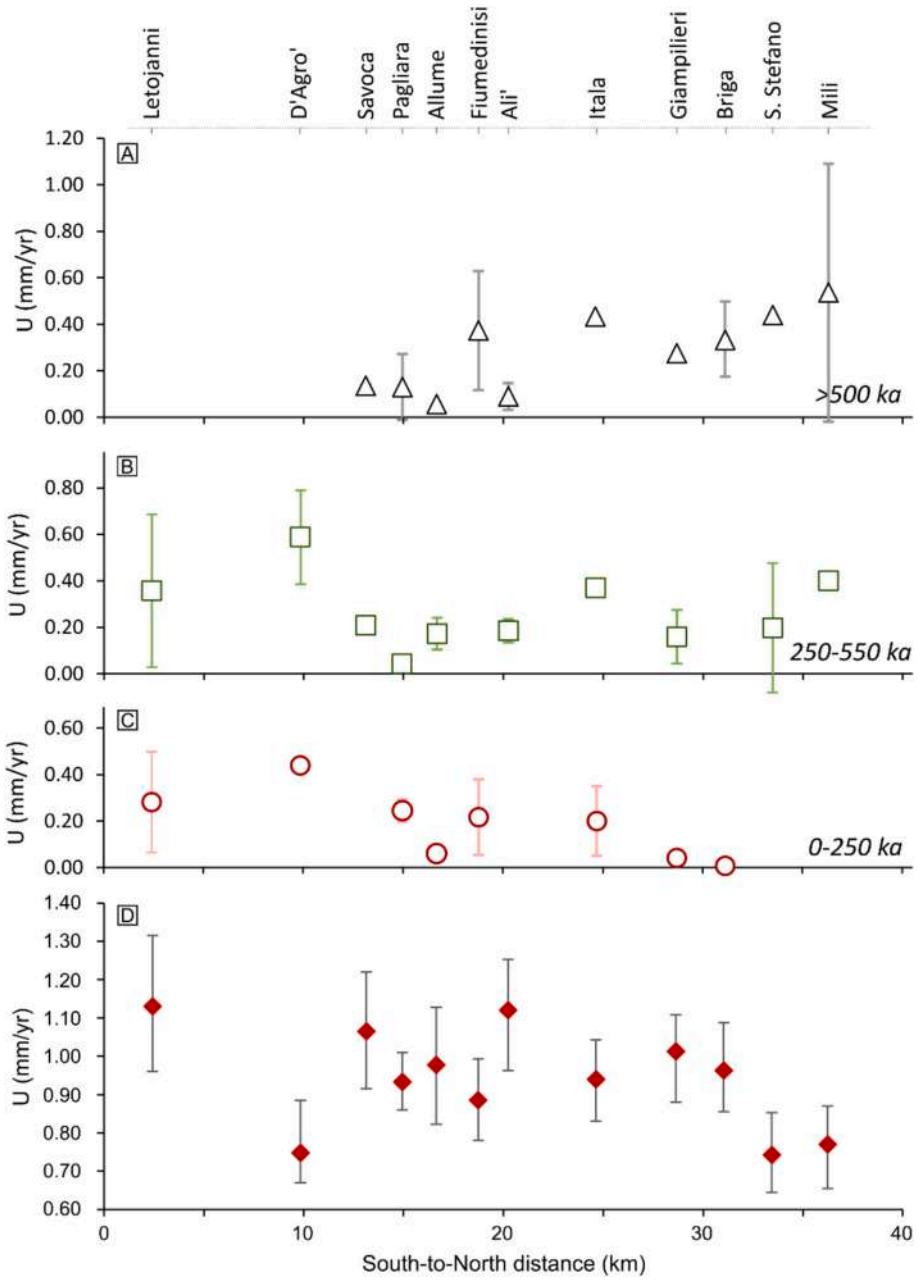

Fig. 4. A–C) Spatial distribution of uplift rate values, net of the background uplift signal, obtained for the different catchments draining the eastern flank of the Peloritani Mts. The different symbols and colors refer to the three different evolutionary stages recognized by river profiles analysis: >500 ka (A), 250–500 ka (B), and 0–250 ka (C). Except for the central sector, where tectonic uplift is almost always recorded, to the south the tectonic signals are generally younger than in the northern counterpart. D) South to North spatial distribution of the whole uplift rate, and the associated errors, provided for each of the analyzed basins and averaged for the <200 ka time frame. The data show a general convex-upward trend, characterized by a, less evident, bimodal distribution.

the SCM analysis. Proceeding to younger psla orders, the VI-to-XIII orders associated with ages 300 ka-to-125 ka show an apparent bimodal distribution of the elevations (Fig. 6B), simulating the same trend of the tdp_2. Finally, the youngest (<125 ka) paleo-shorelines are arranged along an almost symmetrical geometry, similar to the tdp_3, centered in the area of the Allume-Fiumedinisi basins (Fig. 6B).

Differently than the terraced marine surfaces, the psla distribution reveal that the southern sector of the investigated area shows more levels than the northern one, where the psla flight appears more condensed.

Furthermore, I integrated the elevations of the mapped marine terraces with those of the paleo-shorelines, thus obtaining a more complete dataset of paleo-sea level markers in response of a combination of tectonic forcings and sea level changes (Fig. 6C).

Finally, I compared the elevations (m a.s.l.) of the sea level markers mapped by the SCM tool and psla analysis with the modelled marine terraces' inner-edges, predicted using BLF rate data for those sections close to the outlets of the analyzed drainage basins (Table 4 and Table 5) (the target sections are those with headings written in italics red text in Table 3). The spatial distribution of the modelled marine terraces shows an overall trend that matches the general antiformal pattern drawn for the mapped marine terraces (Fig. 7A–G and Fig. 8). Most of the elevations of the modelled marine terraces, either overlaps the mapped ones or falls within their error bars. In some cases, the two datasets largely differ each other, such as in the case of the data modelled for the northernmost sections (Fig. 7A–E), partially for the Pagliara-Allume

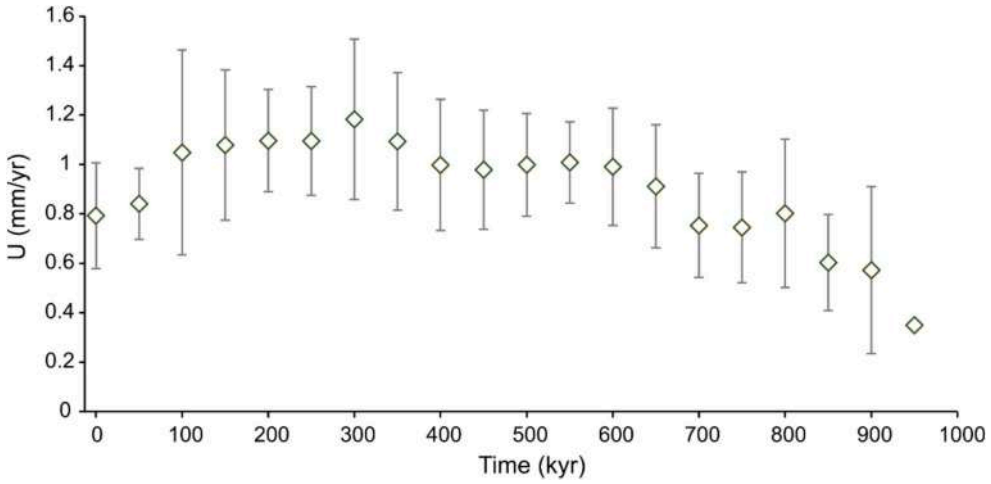

Fig. 5. Time distribution of the average uplift rates for the last ~1Myrs and integrated for the entire study area. The data show a general incremental trend proceeding towards the present, ranging between ~0.4 mm/yr and ~1.2 mm/yr.

Table 3
Marine terraces mapped by using the MAP tool of TerraceM-2 software package. The columns with headings written in italics red text are those associable to the analyzed drainage basins and used to model the marine terraces elevations by applying BLF rate data. The references used to build the marine terraces' age model are marked with asterisks.

MT Order	Age (ka)	S1	S2	S3	S4	*S5*	S6	S7	*S8*	S9	*S10*	*S11*	*S12*	S13	S14	*S15*	S16	S17	S18	*S19*	*S20*
13	***570***		571												684						
12	***520***		515											592							
11	***480***		470								509				534					342	
10	***410***	395	407			448					446			508	499				324	331	320
9	***330***	351	343			415					406			463	424				290	285	
8	***305***				337	346	371		331		351		352	355	346	306			251	252	245
7	***280***	240			270	283			309		301		295	290	261				235	205	210
6	***240***	212					268		239***			250		249	237	226	223	185	175	165	153
5	***200***	156			200		220		199***			198		228	215	181	152	152	140	142	133
4	***125***	107**		141		152			168	167	172	154	157	162	145	132	141	127	112	106	111*
3	***100***	84		110	119	134		121	138	146	144	132	115	116		100	92	93			
2	***80***	40		68		71	71	84	104	108	105	87		84							
1	***60***	29		41				53	60	61	58		63					56			
	Distance (km)	*0*	*1*	*2*	*3*	*5*	*8*	*10*	*12*	*14*	*16*	*19*	*20*	*22*	*23*	*25*	*26*	*27*	*28*	*30*	*36*
	Reference Basin					*Letojanni*		*D'Agro'*	*Savoca*		*Pagliara-Allume*	*Fiumedinisi*	*Ali'*			*Itala*			*Giampilieri*	*Briga*	*Sstefano-Mili*
Legend																					
111*	*Age constrain - Catalano et al. (2003)*																				
156**	*Age constrain - Antonioli et al. (2006)*																				
199***	*Age constrain - Pavano et al. (2024)*																				

basins area (i.e. Section 10), and also for data modelled for the 100 ka time step (Fig. 7G). These latter are mostly lower than the corresponding mapped marine terraces.

4.3. Long-term spatial-temporal variations of the reconstructed tectonic uplift

Based on the dated Late Pleistocene deposits available in literature (Bonfiglio and Violanti, 1983; Bonfiglio, 1991; Bada et al., 1991; Catalano and De Guidi, 2003; Antonioli et al., 2006; Ferranti et al., 2010; Pavano et al., 2024), I associated each of the integrated levels of marine terraces and paleo-shoreline angles with an MIS of the reference global eustatic curve (Waelbroeck et al., 2002).

Then, I defined a general age model that I used to calculate the uplift rate (*U*) variability along each section. Maximum uplift rate's values are shown in the central sector of the studied belt, in accordance with the antiformal distribution of marine markers, with minimum rate reached at both the southern and northern termini. This spatial distribution trend characterizes also the *U* rate calculated for the 330–100 ka marine terraces mapped at target sections (Table 5) (corresponding to the locations of the studied drainage basins).

In more detail, the resulting *U* rate data (Table 6) show that along each section, the landscape recorded a change in tectonic uplift rate, passing from values roughly around the averaged 1.0 mm/yr to values widely ranging between 1.2 mm/yr and 2.2 mm/yr (Table 6). The age at which this switch occurs varies along the study area. In the southern

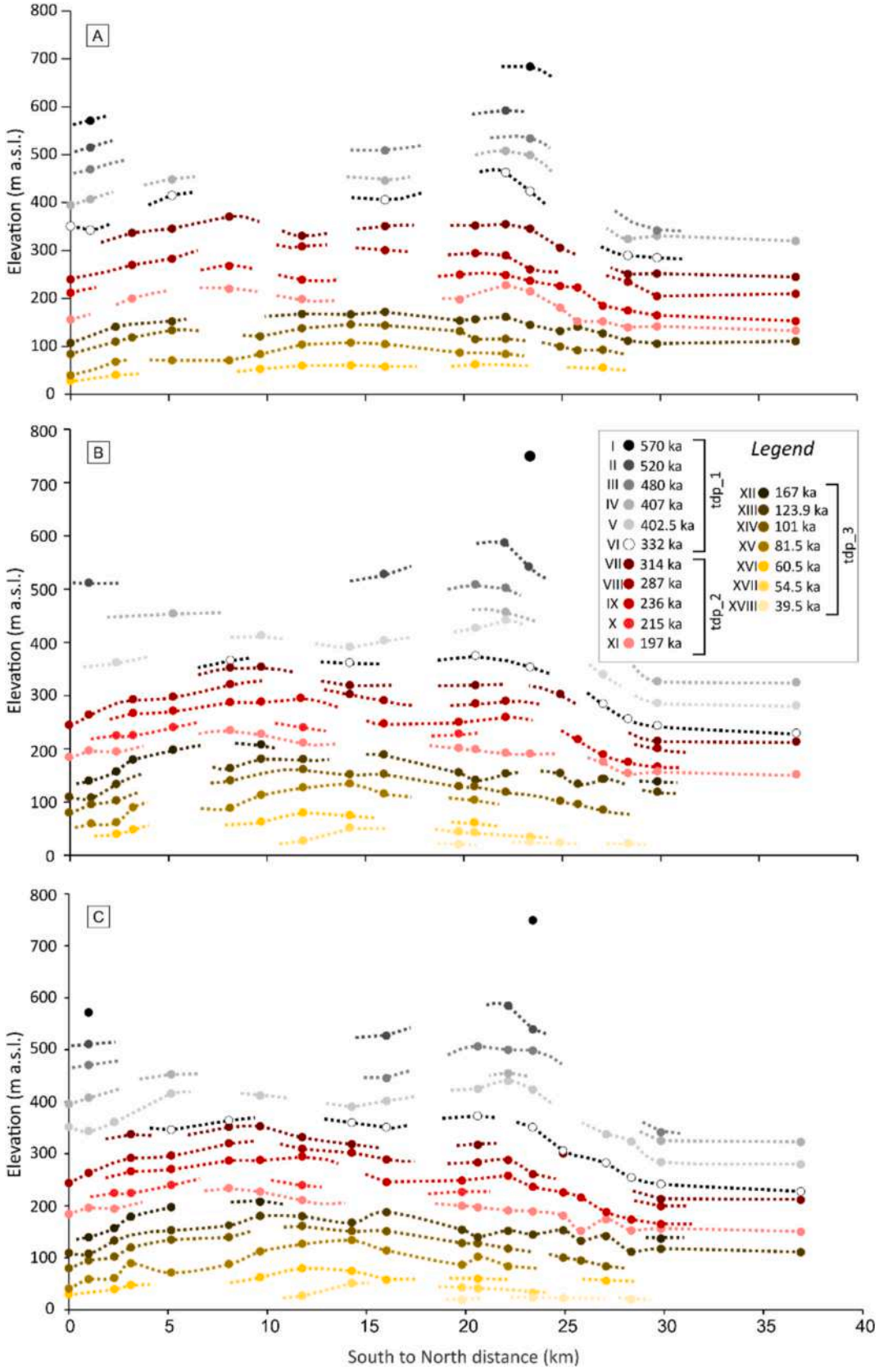

Fig. 6. A) South-to-North spatial distribution of terraced surfaces, mapped by using the MAP tool of TerraceM-2. B) South-to-North spatial distribution of the 18 levels of paleo-shoreline angles manually mapped in TerraceM-2 along selected sections. C) South-to-North spatial distribution of the 18 orders of paleo-shoreline angles integrated with the mapped marine terraced surfaces.

Table 4
Predicted marine terraces' elevations, and associated errors, modelled for the <350 ka time frame in the LEM module of the TerraceM-2 software package (Jara-Muñoz et al., 2019). The model combines the values in uplift rate derived from river profiles inversion analysis with the Waelbroeck et al. (2002) eustatic curve, used as a reference.

MT Order	Age (ka)	MT elevation ± err (m) *Section Letojanni*	MT elevation ± err (m) *Section Savoca*	MT elevation ± err (m) *Section Pagliara-Allume*	MT elevation ± err (m) *Section Fiumedinisi*	MT elevation ± err (m) *Section Ali'*	MT elevation ± err (m) *Section Itala*	MT elevation ± err (m) *Section Briga*	MT elevation ± err (m) *Section S. Stefano-Mili*
	+	79	69	40	39	19	43	36	120
9	***330***	322	351	345	345	392	351	342	335
	–	58	42	52	42	29	59	38	104
	+	76	68	39	35	17	40	34	114
8	***305***	281	316	306	305	358	310	304	293
	–	52	41	48	41	28	53	36	98
	+	71	63	33	32	16	34	29	101
7	***280***	251	295	279	274	337	281	279	260
	–	45	40	42	37	28	47	33	85
	+	62	50	23	28	15	25	24	60
6	***240***	194	258	225	217	296	227	232	201
	–	35	38	27	30	26	33	27	55
	+		40	21	24	12	19	20	
5	***200***		219	182	174	254	186	193	
	–		33	18	21	25	26	23	
	+	37	22	8	16	12	12	15	14
4	***125***	111	141	120	113	162	124	126	104
	–	21	20	10	15	16	13	13	15
	+	29	16	7	12	10	8	10	10
3	***100***	68	85	70	65	101	75	75	58
	–	19	15	7	13	13	10	11	55
	Dist. (km)	*5*	*13*	*16*	*19*	*20*	*25*	*30*	*36*

Table 5
Mapped marine terraces' elevations, and associated errors (+ and - errors are represented by numbers in red and in blue, respectively), for the <350 ka time frame.

MT Data	Age (ka)	S5	S8	S10	S11	S12	S15	S19	S20
	+	6		5					
	330	415		406				285	
	-	6		10					
	+	4	10	0.5		2	0.5	5	3
	305	346	331	351		352	306	252	245
	-	4	9	1		2	1	5	2
	+	3	4	25				8	5
	280	283	309	301		295		205	210
	-	2	4	19				9	8
	+		24		1		12	8	2
	240		239		250		226	165	153
	-		42		1		16	9	4
	+		13		2		4	2	4
	200		199		198		181	142	133
	-		21		2		2	1	5
	+		13	5	0.5	2	6	2	5
	125	152	168	172	154	157	132	106	111
	-		27	3	1	5	7	1	6
	+	19	20	4	4	8			
	100	134	138	144	132	115	100		
	-	20	41	5	7	15			
	Distance (km)	*5*	*13*	*16*	*19*	*20*	*25*	*30*	*36*
		Letojanni	*Savoca*	*Pagliara-Allume*	*Fiumedinisi*	*Ali'*	*Itala*	*Briga*	*S.Stefano-Mili*

sector, from section 1 (near Letojanni basin area) to section 8 (Savoca-Pagliara basins area), the age of the onset of increased tectonic uplift rate passes from 60 ka at section 1, to 170 ka at sections 2–4, up to 240 ka for sections 5–8. Starting from section 9 towards the north, the landscape recorded the onset of higher uplift rates starting from 125 ka, almost constantly up to the northern termini of the fault system, with exceptions for sections 12 and 20 (100 ka), and for sections 16-to-18 (100-to-40 ka). In some cases, these ages are referred to the first recognized marine markers that provides *U* values over the regional component of ~0.8–1 mm/yr, although the onset of faster uplift could be older (Table 6). In particular, sections 12 to 14, roughly corresponding to the Ali'-to-Giampilieri basins area, show an older stage of relatively higher uplift rate, reaching values up to 1.32 mm/yr. Particularly for sections 13 and 14, it is difficult to establish the actual

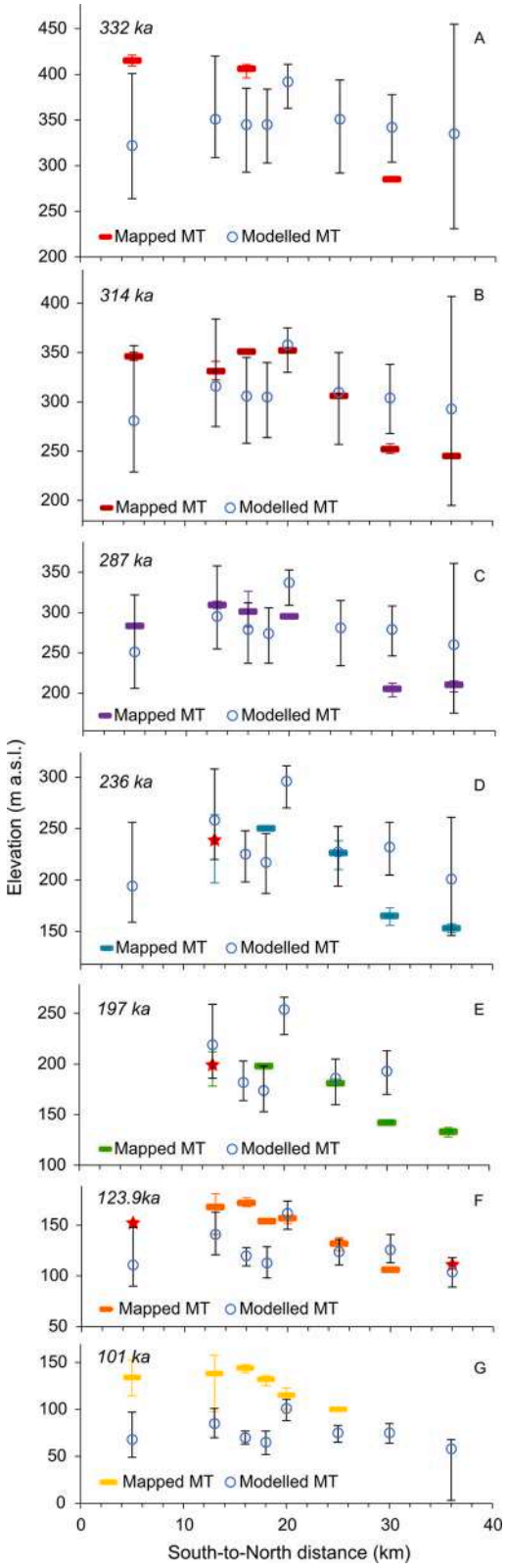

Fig. 7. A–G) Mapped vs. modelled elevations of marine terraces along the eastern coastal belt of Peloritani Mts. The errors associated with the modelled marine terraces elevations derives by propagating in the LEM experiments in TerraceM-2 the uncertainties from the river profiles' inversions. The errors of the mapped marine terraces reflect the variation in elevation of their inner edges, measured in a GIS environment. Red stars indicate those mapped terraces for which I used available data (Catalano and De Guidi, 2003; Antonioli et al., 2006; Pavano et al., 2024) as reference (see the text for more details).

beginning of these high-*U* stage, since the age model built for these marine markers does not go back in time beyond 520 ka. Actually, the BLF histories reconstructed for Ali', Itala, and Giampilieri basins highlight an older peak at about 500–600 ka, thus corroborating the *U* data calculated for sections 13 and 14. Conversely, sections 19 and 20 do not display a net change in *U* around 400–500 ka (Table 6) as pictured by the BLF reconstructions, also due to partial lacking of paleo-sea-level data. Finally, section 11, located in the area of Fiumedinisi basin, shows an increase in *U* for the last 125 ka, which does not have an equivalent in the related BLF history.

5. Discussion

The series of river profile inversions performed for the main catchments draining the eastern flank of the Peloritani Mts. ridge disclosed a fluvial topography repeatedly experiencing base level fall events during the Late Quaternary. In particular, along the investigated area, the results highlight that there was a general north-to-south diachrony in the onset of the reaction of the drainage system to tectonic pulses. It is to note that, since the eustatic contribution to the recorded signal has been almost removed by setting a τ intervals of 50 kyr, I associate the base level fall inputs with discrete tectonic deformation events, thought linked to multiple long-term earthquake cycles occurred along the near-offshore Taormina fault zone.

5.1. Geomorphic time-transgressive response to fault segments activation

The reconstructed BLF histories (Fig. 3 and SI5) provide a general snapshot of the strain partitioning along the Taormina Fault system, portraying a time-transgressive activation of its different portions in response to a southward propagation of crustal strain.

More specifically, the drainage networks responded to the activation of different discrete fault segments belonging to a more complex fault system. This idea is corroborated by the bimodal spatial pattern of some levels of marine terraces and by BLF rate data, which argue for the Taormina Fault as a fault system composed of at least two ~15 km-long main fault strands (Fig. 3, Fig. 4, and Fig. 6): i) the southern one, running from Letojanni-to-Pagliara basins (hereafter Taormina-Capo S. Alessio fault strand - TCfs), and ii) the central-northern one, involving the Pagliara-to-Briga basins (hereafter Ali' fault strand - Afs). These data are only in partial agreement with the fault geometry proposed by De Guidi et al. (2002), qualitatively based on the interpretation of low-resolution bathymetry. However, differently than the authors, the here proposed structural array accounts for a left-stepping, *en-échelon* geometry, with the development of a relay ramp at the Pagliara basin area. This structural model is also qualitatively portrayed by the orientations of many morpho-structures distributed along the studied coastal belt, such as paleo-sea cliffs, fault scarps, and by the distribution of clastic depositional bodies. In particular, the occurrence of the over-fed Pagliara relay-ramp region, where large volumes of clastic delta sediments deposited at least during the last 330 ka (Pavano et al., 2024), are in good agreement with the increase in sediment yield predicted for the central zone after a faults' linkage (He et al., 2021a).

5.2. Dynamics of the Peloritani Mts. ridge's Main Drainage Divide (MDD)

The swath profile across the Peloritani Mts. shows a cross-range asymmetry (Pavano et al., 2016, 2018) that is almost faithfully reproduced by available landscape evolution models (Hoskins et al., 2023) (Fig. 9A). Applied to the study area, this model would suggest the coexistence of uplift (*U*) and advection (*Ad*) gradients across the Peloritani Mts. range. Indeed, the fast-uplifted eastern side of the Peloritani Mts. range shows a topography less concave than the western one and with relatively higher local relief (*LR*) values (Fig. 9A). In addition, according to available models about fault linkage and landscape evolution (He et al., 2021a), the portion of the Peloritani Mts.'

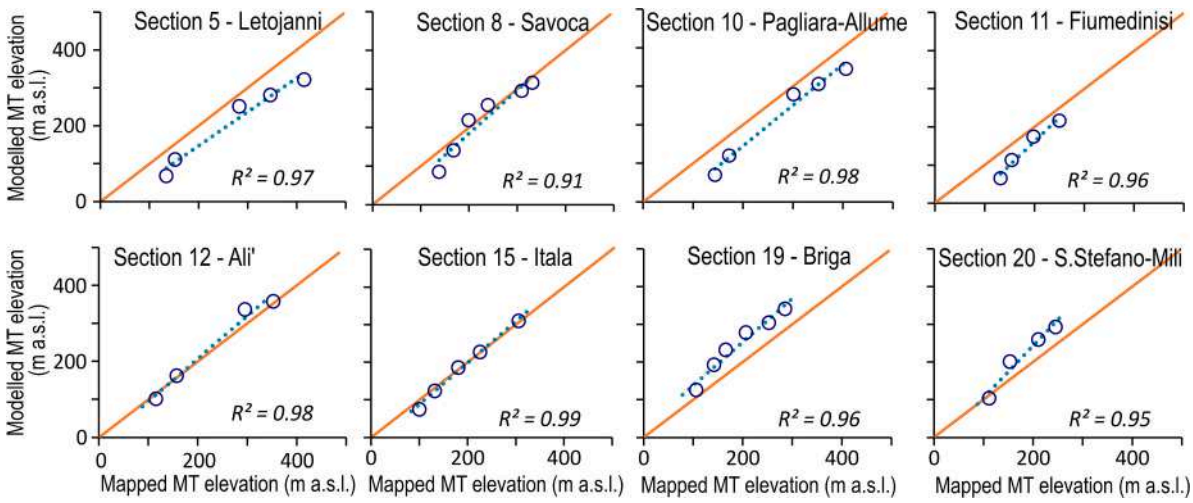

Fig. 8. Plots showing the linear fit between the modelled and the mapped marine terraces' (MT) elevations along target sections, located representatively close to several of the studied drainage basins.

Table 6
Uplift rate values calculated for the integrated dataset of the mapped sea level paleo-markers. Dashed and dotted thick red lines mark main and minor changes in uplift rate, respectively.

P-shrln Order	Age	S1	S2	S3	S4	S5	S6	S7	S8	S9	S10	S11	S12	S13	S14	S15	S16	S17	S18	S19	S20
1	*39.5*											2.06			2.18	2.15			2.09		
2	*54.5*								1.44	1.88		1.75	1.72		1.57						
3	*60.5*	*1.27*		1.43	1.57			1.82	2.10	2.02	*1.75*		1.79					*1.72*			
4	*81.5*	*0.72*	0.94	0.97	1.32	*1.10*	1.30	1.60	1.77	1.86	1.63	*1.30*	1.49	*1.26*							
5	*101*	0.99	1.14	1.21	*1.38*	*1.53*	1.58		1.79	1.70	1.70	1.48	1.47	1.37		1.20	1.15	1.04		*0.21*	*0.21*
6	*123.9*	0.82	0.81	1.02		*1.18*	1.26	1.40	1.39	*1.30*	1.46	1.19	1.08	1.18	*1.12*	1.18	1.02	1.10	*0.85*	0.90	*0.85*
7	*167*		1.13	1.23	1.36	1.47		1.53												1.12	
8	*197*	0.98	1.04	1.03			1.23	1.20	1.12			1.07	1.05	1.02	1.01	*0.97*	*0.82*	0.93	0.82	0.84	0.81
9	*215*			1.06	1.06	1.13			1.13			1.07									
10	*236*				1.17	1.18	1.25	1.26	1.29		1.08	1.09		1.13	*1.04*	*1.00*	0.96	0.84	0.78	0.74	
11	*287*	0.90	0.97		1.07	1.09	1.17		*1.13*	1.11	1.07		1.05	1.06	*0.97*					0.75	
12	*314*				*1.13*		1.17	1.18	*1.11*	1.07			1.07			1.01				0.73	0.73
13	*332*					*1.03*	1.09			1.07	*1.05*		1.11		1.05	*0.91*		0.84	0.76	0.72	0.68
14	*402.5*	*0.86*	*0.84*	0.88		*1.02*		1.01		0.95	0.98		1.04	1.08	*1.04*			0.82	*0.79*	0.69	0.68
15	*407*	*0.95*	*0.98*			1.10								1.10				0.93		0.78	0.78
16	*480*		*0.98*								*0.93*		1.06	1.04	*1.04*						
17	*520*		0.98								1.01			1.13	1.04					*0.66*	
18	570		*1.00*												1.31						
Avg U		0.94	0.98	1.10	1.26	1.18	1.26	1.37	1.43	1.44	1.27	1.38	1.27	1.14	1.21	1.20	0.99	1.03	1.02	0.74	0.68
Dist. (km)		*0*	*1*	*2*	*3*	*5*	*8*	*10*	*12*	*14*	*16*	*19*	*20*	*22*	*23*	*25*	*26*	*27*	*28*	*30*	*36*

divide running roughly from Letojanni basin to Briga basin shows a sinuous trend more than the northernmost sector (Fig. 9B). So, partially following previous results, which would suggest an almost stable MDD for the northeastern Sicily (He et al., 2021b), differences in shape, as well as in Gilbert Metrics and in χ distribution (Forte and Whipple, 2018) (Fig. 9B), between the proximal slope (i.e. the range's slope close to the fault) and the distal slope (i.e. the range's slope far from the fault) (e.g., Hoskins et al., 2023), would suggest a long-term mobility of the Peloritani Mts. MDD. Changes in *U*-vs-*Ad* equilibrium are expected before and after fault strands' linkage and, potentially, even during the main episodes of uplift detected by rivers inversions. Anyway, most of these tectonic inputs are still preserved as upstream-migrating geomorphic signals (Pavano et al., 2016, 2024), with associated modelled ages of ~0.4–0.5 Ma and ~0.25–0.3 Ma (Fig. 3), and thus only partially impacting the MDD's roaming and shape. This means that the across-divide geomorphic disequilibrium is conceivably associated with the early development stage of the two distinct, *en-échelon*-arranged fault segments (i.e. TCfs and Afs), rather than the results of a concluded fault's linkage.

5.3. Models vs observations of paleo-sea level markers

Beyond the definition of the best match between mapped and modelled paleo-shorelines' elevations (e.g., Synchronous Correlation Approach; Roberts et al., 2009, 2013), in this paper the focus is also to explore the potential factors controlling the variable discrepancies in elevation between different datasets of marine paleo-sea level markers.

Uplift rates data from the reconstructed BLF histories for the last 350 ka allowed to numerically model the development of marine terraces in combination with eustasy. The resulting predicted elevations of the shoreline angles partially match those (semi-)automatically mapped by the DEM analysis (Fig. 7), although their overall distribution shows a good linear fit, with R^2 ~0.97 on average (Fig. 8). The mismatching is particularly evident for the marine markers falling in the Savoca-Pagliara basins area (distance of ~15 km in Fig. 7) and for those as young as 100 ka (Fig. 7). This inconsistency cannot depend on the

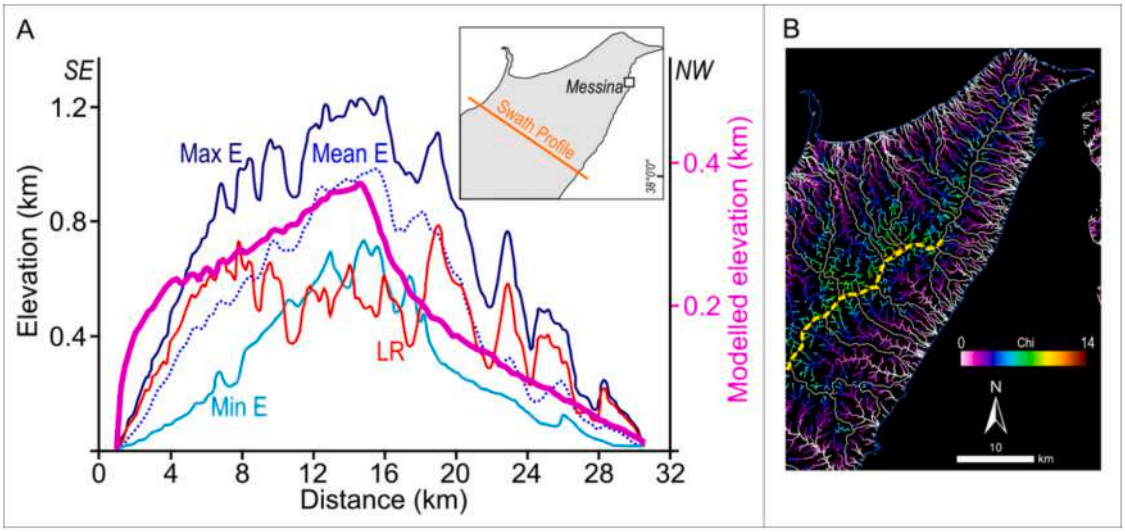

Fig. 9. A) plot showing the main topographic metrics (max, mean, min elevations; Local Relief - LR) sampled across the Peloritani Mts. ridge and plotted together with the modelled elevation for a landscape affected by both tectonic uplift and advection processes' gradients (Hoskins et al., 2023). The inset map shows the trace of the swath profile. B) Chi map of the Peloritani Mts. range. The dashed yellow line marks the portion of the Peloritani Mts. Main Drainage Divide (MDD) with a sinuous trend.

inversion of the downstream over-alluviated portion of the channel, close to the coast. Indeed, recent studies demonstrated that inverting also the short, newly-emerged, alluviated portion of the river profile does not impact on the rivers' linear inversion analysis (Racano et al., 2023; Pavano et al., 2024). This is mainly due to both the very short length of the emerged drainage area (especially like in the case of the eastern Peloritani Mts.) and the very fast transit of knickpoints through an almost straight portion of the channel, hosting highly-erodible loose material. Some of the discrepancies between mapped and modelled elevations of marine terraces could be ascribed to local, limited in time, subsidence episodes. This environmental disturbance could be credited to fault segments' linkage and coalescence, with consequent increase in fault throw, and to the depositional system's evolution, with transfer of sediments from the footwall to the hanging wall of the later-established offshore Taormina Fault, thus overall leading to an increase in accommodation space. This latter, from the perspective of the drainage system, is geomorphically recorded as a system's subsidence. This mechanism could explain why while the marine terracing responded to the tectonic and the eustatic forcings, conversely the drainage system was impacted also by sediments' dynamics.

Differently than the mapped paleo-sea level markers, roughly well matching the elevations reported in previous works (e.g., Catalano and De Guidi, 2003), the elevations of those terraces modelled by using data from river inversions broadly match those predicted by Meschis et al. (2022), especially for those younger than 300-240 ka, and are locally lower than those mapped by Catalano and De Guidi (2003). These discrepancies can be attributed either to the different resolution of the topographic data or to the different geomorphic approaches and tools used to map the marine terraces, as well as the used reference eustatic curve.

5.4. *Spatial-temporal variation model of uplift rate*

The age model defined for the marine paleo-sea level markers (marine terraces and paleo-shoreline angles) allowed exploring the spatio-temporal variations in uplift rate.

The south-to-north distribution of the calculated uplift rates, averaged for each of the 20 target sections and for different time steps, shows

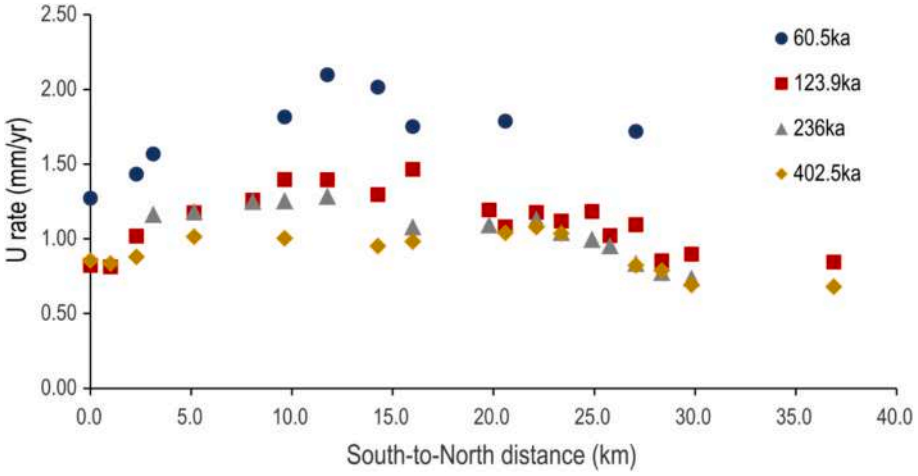

Fig. 10. Plots showing the spatial and temporal distribution of the uplift rate along the eastern Peloritani coastal belt calculated for the integrated dataset of mapped paleo-shoreline angles and marine terraces, and accounting for four time steps: 60.5 ka, 123.9 ka, 236 ka, and 402.5 ka (reference eustatic curve: Waelbroeck et al., 2002).

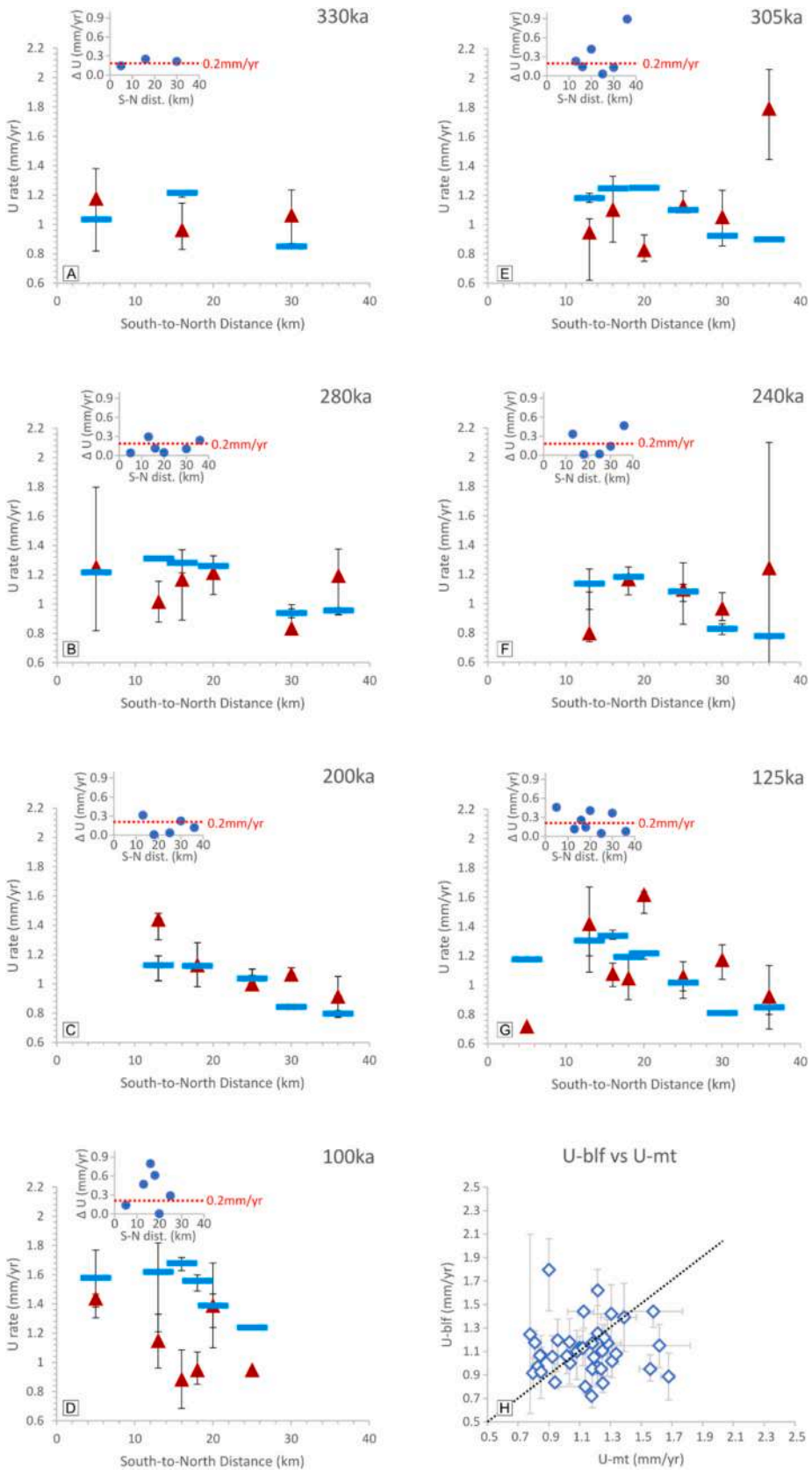

Fig. 11. A–G) Plots showing the uplift rates modelled by marine terrace analysis (light blue bars) vs. those derived by river profile inversion (red tringles) presented for different periods and overall plotted against a 1:1 reference line (H). The inset plots show the distribution of the discrepancies in U (Δ U-rate) computed by comparing the modelled and the observed marine terraces' elevations. The dotted red line refers to the average errors of 0.2 mm/yr associated with the river profiles' inversions.

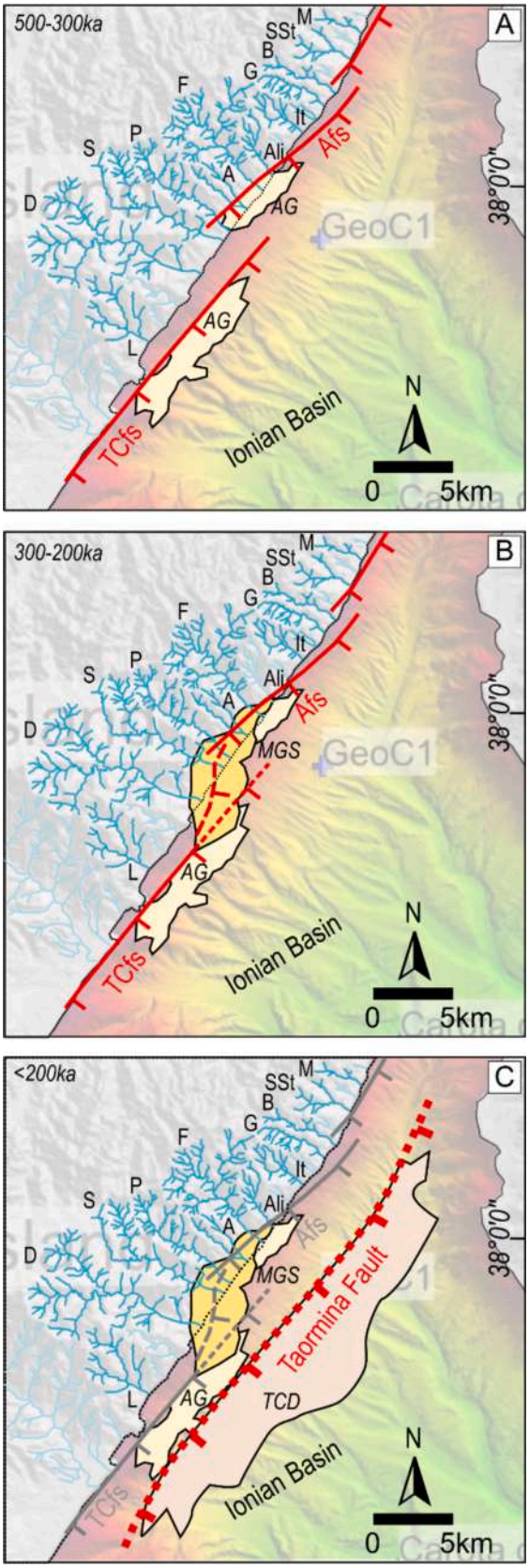

(caption on next column)

Fig. 12. Cartoon showing the schematic morpho-structural evolution of the eastern side of the Peloritani Mts. in three main time steps: 500–300 ka (A), 300–200 ka (B), and <200 ka (C). AG: Allume Gravels; MGS: Messina Gravels and Sands; TCD: Taormina Fault-controlled Clastic Deposits; Afs: Ali' fault strand: TCfs: Taormina-Capo S. Alessio fault strand; Letters refer to the corresponding catchments (see caption of Fig. 3 for reference). Red lines indicate the active faults and the grey lines the non-active ones (long-dashed line where supposed; short-dashed line for deactivating fault; thick dotted line where incipient). The background relief/bathymetry is from SEISMOFAULT project (Billi et al., 2020).

a general antiformal trend (Fig. 10), in accordance with previous works (Catalano and De Guidi, 2003; De Guidi et al., 2003; Catalano et al., 2008; Pavano et al., 2016; Meschis et al., 2022). More in detail, the obtained uplift rate data distribution along the studied sector of the Peloritani Mts. provides further insights about the segmentation of the Taormina Fault system (Table 6). For instance, in the central-northern sector, especially along sections 12, 13 and 14, two main raises in uplift rate are recorded: an older one at ~400–500 ka, and a younger one at ~150–125 ka (see dashed red lines in Table 6). These results would validate the *U* rate data modelled by the river profile inversions (Table 2). Conversely, along the southern sector of the study area (approximatively to the south of Fiumedinisi basin), i.e. along the TCfs, only one main raise in uplift rate emerges (see dashed red line in Table 6). Here, the age of the onset of this increment in uplift rate changes spatially between Section 1 and Section 11. In particular, it is older (~250 ka) at the center (Sections 6–7) and younger towards the two fault strand's termini, thus following the antiformal deformation pattern predicted for the footwall of a normal fault (Gupta and Scholz, 2000; Scholz and Gupta, 2000; Ackermann et al., 2001; Soliva and Benedicto, 2004; Soliva et al., 2006, 2008).

Given the partial temporal overlap between marine terraces and fluvial geomorphic archives, I compared the uplift rate records resulted by both the two independent approaches (Fig. 11A–G), emphasizing the opportunity to use these two data sets to better constrain the uplift rate history. This exercise shows that, although the data are poorly arranged around a 1:1 line (Fig. 11H), most of the discrepancies between the uplift rates obtained by marine terrace analysis and those derived by river profile inversions are in the order of, or lower than 0.2 mm/yr (see inset plots in Fig. 11), which corresponds to the average errors associated with the river profiles' inversions.

5.5. *Strain partitioning, fault interaction and depositional events*

The portrayed structural arrangement is also comforted by field observation on the distribution of the Late Pleistocene clastic deposits (Messina Sands and Gravels, and Allume Gravels formations; Selli, 1978; Bonfiglio and Violanti, 1983; Barrier, 1987; Bonfiglio, 1991; Bada et al., 1991; Carbone et al., 1994; Gargano, 1994; Catalano and Cinque, 1995; Lentini et al., 1995, 2000; Carbone et al., 2008). The deposition of these clastic bodies would have been controlled by the evolution of the two left-stepping *en-échelon* NE-SW-trending fault segments (Afs and TCfs). In such a structural pattern, the two footwall culminations of these two normal fault segments would correspond to the Ali' high, to the north, and to the Taormina-Capo S. Alessio high, to the south (Fig. 12A). The area at the outlets of the Savoca and Pagliara drainage basins correspond to the overlapping zone between the two, potentially dip-down linked (sensu Soliva et al., 2008), normal faults (Fig. 12B), where the relay ramp area hosted the sediments fed by rivers draining the relief of the eastern Peloritani Mts. (Fig. 12B). This structural model is also supported by the ~500-250 ka marine terraces and paleo-shorelines spatial distribution, showing two main highs located around sections 6–7 and 13–14 separated by a sector characterized by marine sea level markers distributed at relatively lower elevations (Fig. 6C).

Following previous works on normal faults' interactions (e.g., Gupta and Scholz, 2000) and on development of fault bends to link two *en-*

échelon arranged faults segments (Accocella et al., 2000), the enhancement of displacement and fault throw rate occurred during <250–200 ka (Tables 1–2 and Fig. 3, Fig. 4, and Fig. 10) and centered at the D'Agro'-Pagliara basins area, can be associated with the soft and moderate-to-strong interaction (sensu Gupta and Scholz, 2000) of TCfs and Afs. The fault segments' linkage could occur after the overcome of local crustal barriers (e.g., relay ramps, transfer zones) represented by the opposition of the elastic forces to the propagation of the extension (Gupta and Scholz, 2000; Soliva and Benedicto, 2004). The stratigraphic expression of this structural evolution sees the faulted and well-deformed older coarse clastic deposits (Allume Gravels), cropping out far to the north in the Fiumedinisi-Ali' basins region, as belonging to the early sedimentary depocenter of the Afs (Fig. 12A). Similarly, early deposition events can be envisaged also offshore the TCfs, as partially imaged by seismic lines showing layered clastic deposits onlapping older bedrock terrains in the offshore of the Capo S. Alessio promontory (Barreca et al., 2019). It is thus reasonable to think that later, once the fault interaction increases and fault linkage proceeded, the depositional depocenter definitely migrated towards the relay ramp zone in the Savoca-Pagliara basins region, hosting younger Messina Sands and Gravel deposits (Fig. 12B–C) (Pavano et al., 2024).

As a final remark, the development of the comprehensive Taormina Fault during the final evolutionary stages could be thought as controlled by either i) deep, lithospheric-scale dynamics, such as slab narrowing and break-off (Argnani, 2009; Chiarabba and Palano, 2017; Maesano et al., 2017; Scarfi' et al., 2018; Pavano and Gallen, 2021), specular to the Apenninic one (Racano et al., 2024; Clementucci et al., 2024), with consequent Mantle inflow and convection reorganization (e.g., Faccenna et al., 2007; Scarfi' et al., 2018; Barreca et al., 2020; Gallen et al., 2023), or ii) the acceleration of the SE-ward migration of the Calabrian Forearc (Rosenbaum and Lister, 2004; Faccenna et al., 2005; Pavano and Gallen, 2021).

6. Conclusions

In the present work I carried out an integrated geomorphic analysis accounting for both river profile inversions, and mapping and modelling of marine terraces and paleo-shoreline angles along the eastern side of the Peloritani Mountains.

The geomorphic approach was applied to investigate the morpho-tectonic evolution of a landscape controlled by a debated offshore fault system (Taormina Fault). The carried study reveals that the early-stage Taormina Fault system was composed of at least two main NNE-SSW-trending, left-stepping *en-échelon* fault segments, activated according to a north-to-south time-transgressive propagation of tectonic deformation. This model is corroborated by: i) the base level fall histories reconstructed for several drainage systems draining the eastern Peloritani Mts. ridge; ii) the altimetric distribution of several orders of marine paleo-sea level markers mapped along the study area; iii) relief analysis, in good agreement with data from independent, published landscape evolution model experiments.

The river inversions' results allow to discretize the study area into three main sectors: the northernmost one, corresponding to the area of S. Stefano and Mili basins, could represent a landscape controlled by a northern fault segment not studied in the present work and strictly connected to the structural setting controlling the Messina Strait area; the central-northern sector, centered at Ali' high, experiencing at least two main tectonic pulses at about 400–500 ka (rate > ~1.2 mm/yr) and 250–300 ka (rate > ~1.4–1.5 mm/yr); the southern sector, roughly centered at the Taormina-Capo S. Alessio area, with the fluvial system recording only the youngest tectonic pulse <300 ka.

This strain partitioning evolutionary model (Fig. 12) is also provided by analyzing the paleo-sea level markers and by investigating the spatial-temporal distribution of the resulting uplift rates. During an early stage (~500–300 ka), higher uplift rates (>1.2 mm/yr) focus in correspondence of the central-northern sector, due to tectonic activity along the Ali' fault strand (Afs), which also controlled the Allume Gravel clastic deposition; later, during the 300-200 ka time frame, the southern sector experiences faster uplift (>1.3–1.4 mm/yr) due to deformation along the Taormina-Capo S. Alessio fault strand (TCfs), potentially followed (<200 ka) by the linkage between the two fault segments, and the deposition of large volume of clastic deposits (Messina Sands and Gravels) (Pavano et al., 2024) in the relay ramp area at the outlets of Savoca-Pagliara basins. Finally, overall the data suggest a subsequent stage characterized by the development of a comprehensive fault, controlling the general antiformal deformtation pattern of the Peloritani Mts. ridge.

The study also highlights how this tectonic evolution, together with advection processes, had also an impact on the general geomorphic evolution of the Peloritani Mts. ridge, such as the long-term dynamics of the main drainage divide.

As a conclusive remark, the data obtained and interpreted in the present study point out how the multiapproach analysis and the integration of different geomorphic data records could help in extending the knowledge about the morpho-tectonic evolution of a region. Deformation models built exploring drainage systems evolution can, thus, contribute in bridging the age resolution gap between models resulting from paleo-sea level markers analyses (10^3–10^5 yrs) and those, longer, obtained by applying classical geological approach (10^6 yrs).

Supplementary data to this article can be found online at https://doi.org/10.1016/j.geomorph.2024.109583.

CRediT authorship contribution statement

F. Pavano: Writing – review & editing, Writing – original draft, Visualization, Validation, Supervision, Resources, Methodology, Investigation, Formal analysis, Data curation, Conceptualization.

Declaration of competing interest

The authors declare that they have no known competing financial interests or personal relationships that could have appeared to influence the work reported in this paper.

Acknowledgments

The author would like to thank the Associate Editor Jing Liu-Zeng for the editorial handling, and two anonymous reviewers for their helpful and constructive comments that improved the earlier version of this paper. The author wants also to thank Dr. Julius Jara-Muñoz for tips about using TerraceM-2 software's tools. The present study was supported by the NSF-EAR-Tectonics program, in the frame of the project TESPRESSO (Tectonic Encoding, Shredding and Propagation of Environmental Signals as Surface Observables), award #1904262 (P.I. Frank J. Pazzaglia), and by the National Recovery and Resilience Plan (NRRP) RETURN (multi-Risk sciEnce for resilienT commUnities undeR a changiNg climate) Project PE_00000005. The study also benefited from the support from the Department of Earth Sciences, Environment and Resources of the University of Naples Federico II.

Data availability

Data will be made available on request.

References

Accocella, V., Gudmundsson, A., Funiciello, R., 2000. Interaction and linkage of extension fractures and normal faults: examples from rift zone of Iceland. J. Struct. Geol. 22, 1233–1246.

Ackermann, R.V., Schlische, R.W., Withjack, M.O., 2001. The geometric and statistical evolution of normal fault systems: an experimental study of the effects of mechanical layer thickness on scaling laws. Journal of Structural Geology 23, 1803–1819.

Aloisi, M., Bruno, V., Cannavo', F., Ferranti, L., Mattia, M., Monaco, C., Palano, M., 2013. Are the source models of theM7.1 1908 Messina Straits earthquake reliable? Insights from a novel inversion and a sensitivity analysis of levelling data. Geophys. J. Int. 192, 1025–1041. https://doi.org/10.1093/gji/ggs062, 2013.

Amodio-Morelli, L., Bonari, G., Colonna, V., Dietrich, D., Giunta, G., Ippolito, F., Liguori, V., Lorenzoni, S., Paglionico, A., Perrone, V., Piccarreta, G., Russo, M., Scandone, P., Zanettin-Lorenzoni, E., Zappetta, A., 1976. L'Arco Calabro-peloritano nell'orogene appenninico-maghrebide. Mem. Soc. Geol. Ital. 17, 1–60.

Antonioli, F., Kershaw, S., Renda, P., Rust, D., Belluomini, G., Cerasoli, M., Radtke, U., Silenzi, S., 2006. Elevation of the last interglacial highstand in Sicily (Italy): a benchmark of coastal tectonics. Quat. Int. 145–146, 3–18.

Antonioli, F., Furlani, S., Montagna, P., Stocchi, P., 2021. The use of submerged speleothems for sea level studies in the Mediterranean Sea: a new perspective using Glacial Isostatic Adjustment (GIA). Geosciences 11, 77. https://doi.org/10.3390/geosciences11020077.

Argnani, A., 2009. Evolution of the southern Tyrrhenian slab tear and active tectonics along the western edge of the Tyrrhenian subducted slab. In: Van Hinsbergen, D.J.J., Edwards, M.A., Govers, R. (Eds.), Collision and Collapse at the Africa–Arabia–Eurasia Subduction Zone, The Geological Society, London, Special Publications, 311, pp. 193–212. https://doi.org/10.1144/SP311.7.

Argnani, A., Bonazzi, C., 2005. Malta Escarpment fault zone offshore eastern Sicily: Pliocene-Quaternary tectonic evolution based on new multichannel seismic data. Tectonics 24, TC4009. https://doi.org/10.1029/2004TC001656.

Argnani, A., Brancolini, G., Bonazzi, C., Rovere, M., Accaino, F., Zgur, F., Lodolo, E., 2009. The results of the Taormina 2006 seismic survey: possible implications for active tectonics in the Messina Straits. Tectonophysics 476, 159–169.

Azzaro, R., Bernardini, F., Camassi, R., Castelli, V., 2007. The 1780 seismic sequence in NE Sicily (Italy): shifting an underestimated and mislocated earthquake to a seismically low rate zone. Nat. Hazards 42, 149–167.

Bada, J.L., Belluomini, G., Bonfiglio, L., Branca, M., Burgio, E., Delitalia, L., 1991. Isoleucin epimerization ages of quaternary mammals from Sicily. Il Quaternario 4 (1), 49–54.

Barreca, G., Scarfì, L., Gross, F., Monaco, C., De Guidi, G., 2019. Fault pattern and seismotectonic potential at the south-western edge of the Ionian Subduction system (southern Italy): new field and geophysical constraints. Tectonophysics 761, 31–45.

Barreca, G., Branca, S., Corsaro, R.A., Scarfì, L., Cannavò, F., Aloisi, M., Monaco, C., Faccenna, C., 2020. Slab detachment, mantle flow, and crustal collision in eastern Sicily (southern Italy): implications on Mount Etna volcanism. Tectonics 39, e2020TC006188. https://doi.org/10.1029/2020TC006188.

Barrier, P., 1987. Stratigraphie des dépots pliocènes et quaternaires du Detroit de Messine (Italie). Documents et travaux de l'Institut Géologique Albert de Lapparent 11, 59–81.

Bianca, M., Monaco, C., Tortorici, L., Cernobori, L., 1999. Quaternary normal faulting in southeastern Sicily (Italy): a seismic source for the 1693 large earthquake. Geophys. J. Int. 139, 370–394.

Billi, A., Presti, D., Orecchio, B., Faccenna, C., Neri, G., 2010. Incipient extension along the active convergent margin of Nubia in Sicily, Italy: Cefalù–Etna seismic zone. Tectonics 29, TC4026. https://doi.org/10.1029/2009TC002559.

Billi, A., Cuffaro, M., Beranzoli, L., Bigi, S., Bosman, A., Caruso, C., Conti, A., Corbo, A., Costanza, A., D'Anna, G., De Caro, M., Doglioni, C., Embriaco, D., Fertitta, G., Frugoni, F., Gasperini, L., Italiano, F., Lazzaro, G., Ligi, M., Martorelli, E., Monna, S., Montuori, C., Nigrelli, A., Passafiume, G., Petracchini, L., Petricca, P., Polonia, A., Proietti, G., Ruggiero, L., Sgroi, T., Tartarello, M.C., 2020. The SEISMOFAULTS project: first surveys and preliminary results for the Ionian Sea area, southern Italy. Ann. Geophys. 63 (3), SE326. https://doi.org/10.4401/ag-8171.

Bintanja, R., van de Wal, R.S.W., Oerlemans, J., 2005. Modelled atmospheric temperatures and global sea levels over the past million years. Nature 437 (7055), 125–128. https://doi.org/10.1038/nature03975.

Bloom, A.L., Yonekura, N., 1985. Coastal terraces generated by sea-level change and tectonic uplift. In: Woldenberg, M.J. (Ed.), Models in Geomorphology, Binghamton Symposia in Geomorphology: International Series, 14, pp. 139–154. Binghamton, New York.

Boccaletti, M., Nicolich, R., Tortorici, L., 1990. New data and hypothesis on the development of the Tyrrhenian basin. Paleogeog. Paleoclimat. Paleoecol. 77, 15–40.

Bonfiglio, L., 1991. Correlazioni tra depositi a mammiferi, depositi marini, linee di costa e terrazzi medio e tardo-pleistocenici nella Sicilia orientale. Il Quaternario 4 (1b), 205–214.

Bonfiglio, L., Violanti, D., 1983. Prima segnalazione di Tirreniano ed evoluzione pleistocenica del Capo Peloro (Sicilia nord-orientale). Geogr. Fis. Din. Quat. 6, 3–15.

Bowles, C.J., Cowgill, E., 2012. Discovering marine terraces using airborne LiDAR along the Mendocino-Sonoma coast, northern California. Geosphere 8 (2), 386–402. https://doi.org/10.1130/GES00702.1.

Buleo Tebar, V., Bonasera, M., Racano, S., Fubelli, G., 2024. River linear inversion to assess drainage base-level fall history in North-western Apennines and implications on the Alessandria Basin tectonic activity. Geomorphology 462, 109327. https://doi.org/10.1016/j.geomorph.2024.109327.

Cammarata, L., Catalano, S., Gambino, S., Palano, M., Pavano, F., Romagnoli, G., Scaltrito, A., Tortorici, G., 2018. Seismological and structural constraints on the 2011–2013, Mmax 4.6 seismic sequence at the south-eastern edge of the Calabrian arc (North-eastern Sicily, Italy). Tectonophysics 723, 56–67.

Carbone, S., Catalano, S., Lentini, F., Vinci, G., 1994. Carta Geologica dei Monti di Taormina (Sicilia nord-orientale). Scala 1:25.000. S.EL.CA, Firenze.

Carbone, S., Messina, A., Lentini, F., 2008. Note Illustrative del F. 601 "Messina-Reggio di Calabria" della Carta Geologica d'Italia alla scala 1:50.000. APAT. S.EL.CA, p. 179.

Catalano, S., Cinque, A., 1995. L'evoluzione neotettonica dei Peloritani settentrionali (Sicilia nord-orientale): il contributo di una analisi geomorfologica preliminare. Studi Geol. Camerti Spec. 1995/2, 113–123.

Catalano, S., De Guidi, G., 2003. Late Quaternary uplift of northeastern Sicily: relation with the active normal faulting deformation. J. Geodyn. 36, 445–467.

Catalano, S., Di Stefano, A., 1997. Sollevamento e tettogenesi Pleistocenica lungo il margine tirrenico dei Monti Peloritani: integrazione dei dati geomorfologici, strutturali e biostratigrafici: Il. Quaternario 10, 337–342.

Catalano, S., De Guidi, G., Monaco, C., Tortorici, G., Tortorici, L., 2003. Long-term behavior of the late Quaternary normal faults in the Straits of Messina area (Calabrian arc): structural and morphological constraints. Quat. Int. 101, 81–91. https://doi.org/10.1016/S1040-6182(02)00091-5.

Catalano, S., De Guidi, G., Monaco, C., Tortorici, G., Tortorici, L., 2008. Active faulting and seismicity along the Siculo-Calabrian rift zone. Tectonophysics 453, 177–192.

Catalano, S., Romagnoli, G., Tortorici, G., 2010. Kinematics and dynamics of the Late Quaternary rift-flank deformation in the Hyblean Plateau (SE Sicily). Tectonophysics 486, 1–14. https://doi.org/10.1016/j.tecto.2010.01.013.

Catalano, S., Pavano, F., Romagnoli, G., Tortorici, G., 2012. Active tectonic along the Nebrodi–Peloritani bounday (NE Sicily): a new potential seismogenic source. Rend. Online Soc. Geol. Ital. 22, 44–47.

Catalano, S., Cirrincione, R., Mazzoleni, P., Pavano, F., Pezzino, A., Romagnoli, G., Tortorici, G., 2018. The effects of a Meso-Alpine collision event on the tectono-metamorphic evolution of the Peloritani mountain belt (eastern Sicily, southern Italy). Geol. Mag. 155 (2), 422–437.

Chiarabba, C., Palano, M., 2017. Progressive migration of slab break-off along the southern Tyrrhenianplate boundary: constraints for the present day kinematics. J. Geodyn. 105, 51–61. https://doi.org/10.1016/j.jog.2017.01.006.

Cirrincione, R., Pezzino, A., 1994. Nuovi dati strutturali sulle successioni mesozoiche metamorfiche dei M. Peloritani orientali. Bollettino della Società Geologica Italiana 113, 195–203.

Clementucci, R., Lanari, R., Faccenna, C., Crosetto, S., Reitano, R., Zoppis, G., Ballato, P., 2024. Morpho-tectonic evolution of the Southern Apennines and Calabrian Arc: insights from Pollino range and surrounding extensional intermontane basins. Tectonics 43, e2023TC008002. https://doi.org/10.1029/2023TC008002.

Crosetto, S., De Montserrat, A., Oncken, O., 2024. Uplifted Pleistocene marine terraces at active margins: modeling reveals the effects of sea reoccupation and coseismic uplift on uplift rate calculation. Geochem. Geophys. Geosyst. 25, e2023GC011036. https://doi.org/10.1029/2023GC01136.

Cyr, A.J., Granger, D.E., Olivetti, V., Molin, P., 2010. Quantifying rock uplift rates using channel steepness and cosmogenic nuclide–determined erosion rates: examples from northern and southern Italy. Lithosphere 2 (3), 188–198.

De Guidi, G., Catalano, S., Monaco, C., Tortorici, L., Di Stefano, A., 2002. Long-term effects of late Quaternary normal faulting in southern Calabria and eastern Sicily. Studi Geologici Camerti, Nuova Serie 1, 79–93.

De Guidi, G., Catalano, S., Monaco, C., Tortorici, L., 2003. Morphological evidence of Holocene coseismic deformation in the Taormina region (NE Sicily). Journal of Geodynamics 36, 193–211.

Dewey, J.F., Helman, M.L., Turco, E., Hutton, D.H.W., Knott, S.D., 1989. Kinematics of the western Mediterranean. Alpine Tectonics. Geol. Soc. Spec. Publ. 45, 265–283.

DiBiase, R.A., Whipple, K.X., Heimsath, A.M., Ouimet, W.B., 2010. Landscape form and millennial erosion rates in the San Gabriel Mountains. Earth and Planetary Science Letters 289, 134–144. https://doi.org/10.1016/j.epsl.2009.10.036.

Di Stefano, A., Longhitano, S.G., 2009. Tectonics and sedimentation of the Lower and Middle Pleistocene mixed siliciclastic/bioclastic sedimentary successions of the Ionian Peloritani Mts (NE Sicily, Southern Italy): the onset of opening of the Messina Strait. Cent. Eur. J. Geosci. 1 (1), 33–62. https://doi.org/10.2478/v10085-009-0002-y.

DISS Working Group, 2021. Database of Individual Seismogenic Sources (DISS), Version 3.3.0: A Compilation of Potential Sources for Earthquakes Larger than M 5.5 in Italy and Surrounding Areas. Istituto Nazionale di Geofisica e Vulcanologia (INGV). https://doi.org/10.13127/diss3.3.0.

Dorsey, R.J., Longhitano, S.G., Chiarella, D., 2023. Structure and morphology of an active conjugate relay zone, Messina Strait, southern Italy. Basin Res. 36, e12818. https://doi.org/10.1111/bre.12818.

Faccenna, C., Civetta, L., D'Antonio, M., Funiciello, F., Margheriti, L., Piromallo, C., 2005. Constraints on mantle circulation around the deforming Calabrian slab. Geophys. Res. Lett. 32, L06311. https://doi.org/10.1029/2004GL021874.

Faccenna, C., Funiciello, F., Civetta, L., D'Antonio, M., Moroni, M., Piromallo, C., 2007. Slab disruption, mantle circulation, and the opening of the Tyrrhenian basins. In: Beccaluva, L., Bianchini, G., Wilson, M. (Eds.), Cenozoic Volcanism in the Mediterranean Area: Geological Society of America Special Paper, 418, pp. 153–169. https://doi.org/10.1130/2007.2418(08.

Faccenna, C., Molin, P., Orecchio, B., Olivetti, V., Bellier, O., Funiciello, F., Minelli, L., Piromallo, C., Billi, A., 2011. Topography of the Calabria subduction zone (southern Italy): clues for the origin of Mt. Etna. Tectonics 30, TC1003.

Faccenna, C., Becker, T.W., Auer, L., Billi, A., Boschi, L., Brun, J.P., Capitanio, F.A., Funiciello, F., Horvàth, F., Jolivet, L., Piromallo, C., Royden, L., Rossetti, F., Serpelloni, E., 2014. Mantle dynamics in the Mediterranean. Rev. Geophys. 52, 283–332. https://doi.org/10.1002/2013RG000444.

Falcone, G., Mendicelli, A., Mori, F., Fabozzi, S., Moscatelli, M., Occhipinti, G., Peronace, E., 2020. A simplified analysis of the total seismic hazard in Italy. Eng. Geol. 267, 105511. https://doi.org/10.1016/j.enggeo.2020.105511.

Ferranti, L., Antonioli, F., Mauzc, B., Amorosi, A., Dai Prab, G., Mastronuzzi, G., Monaco, C., Orru', P., Pappalardo, M., Radtkei, U., Renda, P., Romano, P., Sanso', P., Verrubbi, V., 2006. Markers of the last interglacial sea-level high stand along the coast of Italy: tectonic implications. Quat. Int. 145–146, 30–54.

Ferranti, L., Antonioli, F., Anzidei, M., Monaco, C., Stocchi, P., 2010. The timescale and spatial extent of recent vertical tectonic motions in Italy: Insights from relative sea-level changes studies. J. Virtual Explor. 36, 23. https://doi.org/10.3809/jvirtex.2010.00255.

Ferranti, L., Antonioli, F., Scicchitano, G., Spampinato, C.R., 2017. Uplifted late Holocene shorelines along the coasts of the Calabrian Arc: geodynamic and seismotectonic implications. Ital. J. Geosci. 136 (3), 454–470. https://doi.org/10.3301/IJG.2017.13.

Fisher, J.A., Pazzaglia, F.J., Anastasio, D.J., Gallen, S.F., 2022. Linear inversion of fluvial topography in the northern Apennines: comparison of base-level fall to crustal shortening. Tectonics 41, e2022TC007379. https://doi.org/10.1029/2022TC007379.

Forte, A.M., Whipple, K.X., 2018. Criteria and tools for determining drainage divide stability. Earth Planet. Sci. Lett. 493, 102–117.

Forte, A.M., Whipple, K.X., 2019. Short communication: short communication: the Topographic Analysis Kit (TAK) for TopoToolbox. Earth Surf. Dyn. 7, 87–95. https://doi.org/10.5194/esurf-7-87-2019.

Foti, A., Pavano, F., Romagnoli, G., Tortorici, G., Catalano, S., 2023. Structural geology of the eastern termination of the Mt. Kumeta-Alcantara line (NE sicily, Italy). Journal of Maps 19 (1), 2179436. https://doi.org/10.1080/17445647.2023.2179436.

Gailleton, B., Mudd, S.M., Clubb, F.J., Grieve, S.W.D., Hurst, M.D., 2021. Impact of changing concavity indices on channel steepness and divide migration metrics. JGR Earth Surface 126, e2020JF006060. https://doi.org/10.1029/2020JF006060.

Gallen, S.F., 2018. Lithologic controls on landscape dynamics and aquatic species evolution in post-orogenic mountains. Earth Planet. Sci. Lett. 493, 150–160. https://doi.org/10.1016/j.epsl.2018.04.029.

Gallen, S.F., Fernández-Blanco, D., 2021. A new data-driven Bayesian inversion of fluvial topography clarifies the tectonic history of the corinth rift and reveals a channel steepness threshold. J. Geophys. Res. Earth, e2020JF005651. https://doi.org/10.1029/2020JF005651.

Gallen, S.F., Seymour, N.M., Glotzbach, C., Stockli, D.F., O'Sullivan, P., 2023. Calabrian forearc uplift paced by slab–mantle interactions during subduction retreat. Nat. Geosci. 16 (6), 1–8. https://doi.org/10.1038/s41561-023-01185-4.

Gargano, C., 1994. Carta geologica della zona di Messina Monti Peloritani Sicilia NE. Scala 1:25.000. S.El.CA.

Ghisetti, F., 1979. Relazioni tra strutture e fasi trascorrenti e distensive lungo i sistemi Messina-Fiumefreddo, Tindari-Letojanni e Alia-Malvagna (Sicilia nord-orientale): uno studio microtettonico. Geol. Romana 18, 23–58.

Goren, L., Fox, M., Willett, S.D., 2014. Tectonics from fluvial topography using formal linear inversion: theory and applications to the Inyo Mountains, California. J. Geophys. Res. Earth 119 (8), 1651–1681. https://doi.org/10.1002/2014JF003079.

Goswami, R., Brocklehurst, S.H., Mitchell, N.C., 2012. Erosion of a tectonically uplifting coastal landscape, NE Sicily, Italy. Geomorphology 171–172, 112–126. https://doi.org/10.1016/j.geomorph.2012.05.011.

Gupta, A., Scholz, C.H., 2000. A model of normal fault interaction based on observations and theory. Journal of Structural Geology 22, 865–879.

Hancock, G.S., Anderson, R.S., Whipple, K.X., 1998. Beyond power: Bedrock river incision process and form. In: Tinkler, K.J., Wohl, E.E. (Eds.), Rivers Over Rock: Fluvial Processes in Bedrock Channels, American Geophysical Union Geophysical Monograph, 107, pp. 35–60. https://doi.org/10.1029/GM107p0035.

Harel, M.-A., Mudd, S.M., Attal, M., 2016. Global analysis of the stream power law parameters based on worldwide 10Be denudation rates. Geomorphology 268, 184–196. https://doi.org/10.1016/j.geomorph.2016.05.035.

He, C., Yang, C.-J., Turowski, J.M., Rao, G., Roda-Boluda, D.C., Yuan, X.P., 2021a. Constraining tectonic uplift and advection from the main drainage divide of a mountain belt. Nat. Commun. 12, 544. https://doi.org/10.1038/s41467-020-20748-2.

He, C., Yang, C.-J., Rao, G., Roda-Boluda, D.C., Yuanb, X., Yang, R., Gao, L., Zhang, Li, 2021b. Landscape response to normal fault linkage: insights from numerical modeling. Geomorphology 388, 107796. https://doi.org/10.1016/j.geomorph.2021.107796.

Hoskins, A.M., Attal, M., Mudd, S.M., Castillo, M., 2023. Topographic response to horizontal advection in normal fault-bound mountain ranges. J. Geophys. Res. Earth 128 (8), e2023JF007126. https://doi.org/10.1029/2023JF007126.

Jara-Muñoz, J., Melnick, D., Brill, D., Strecker, M.R., 2015. Segmentation of the 2010 Maule Chile earthquake rupture from a joint analysis of uplifted marine terraces and seismic-cycle deformation patterns. Quaternary Science Reviews 113, 171–192. https://doi.org/10.1016/j.quascirev.2015.01.005.

Jara-Muñoz, J., Melnick, D., Strecker, M.R., 2016. TerraceM: a MATLAB® tool to analyze marine and lacustrine terraces using high-resolution topography. Geosphere 12 (1), 176–195. https://doi.org/10.1130/ges01208.1.

Jara-Muñoz, J., Melnick, D., Zambrano, P., Rietbrock, A., González, J., Argandoña, B., Strecker, M.R., 2017. Quantifying offshore fore-arc deformation and splay-fault slip using drowned Pleistocene shorelines, Arauco Bay, Chile. J. Geophys. Res. Solid Earth 122, 4529–4558. https://doi.org/10.1002/2016JB013339.

Jara-Muñoz, J., Melnick, D., Pedoja, K., Strecker, M.R., 2019. TerraceM-2: a Matlab R interface for mapping and modeling marine and lacustrine terraces. Front. Earth Sci. 7, 255. https://doi.org/10.3389/feart.2019.00255.

Kelsey, H.M., 1990. Late quaternary deformation of marine terraces on the Cascadia subduction zone near Cape Blanco, Oregon. Tectonics 9 (5), 983–1014. https://doi.org/10.1029/TC009i005p00983.

Kelsey, H.M., Bockheim, J.G., 1994. Coastal landscape evolution as a function of eustasy and surface uplift rate, Cascadia margin, Southern Oregon. GSA Bull. 106, 840–854.

Lague, D., 2014. The stream power river incision model: evidence, theory and beyond. Earth Surf. Process. Landf. 39 (1), 38–61. https://doi.org/10.1002/esp.3462.

Lajoie, K.R., 1986. Coastal tectonics. In: Active Tectonics. National Academic Press, Washington, DC, pp. 95–124.

Lentini, F., Carbone, S., Catalano, S., Grasso, M., 1995. Principali lineamenti strutturali della Sicilia nord-orientale. Studi Geol. Camerti 1995 (2), 319–329 (special issue).

Lentini, F., Carbone, S., Catalano, S., Grasso, M., 1996. Elementi per la ricostruzione del quadro strutturale della Sicilia orientale: Memorie della Societa Geologica Italiana, 51, 179–195.

Lentini, F., Catalano, S., Carbone, S., 2000. In: S.EL.CA (Ed.), Nota illustrativa della Carta geologica della Provincia di Messina (Sicilia Nord-Orientale), scala 1:50.000. Firenze, 70 pp.

Lentini, F., Vezzani, L., 1975. Le unità meso-cenozoiche della copertura sedimentaria del basamento cristallino peloritano (Sicilia nord-orientale). Bollettino della Società Geologica Italiana 94, 537–554.

Maesano, F.E., Tiberti, M.M., Basili, R., 2017. The Calabrian Arc: three-dimensional modelling of the subduction interface. Sci. Rep. 7, 8887. https://doi.org/10.1038/s41598-017-09074-8.

Malatesta, L.C., Bruhat, L., Finnegan, N.J., Olive, J.A.L., 2021. Co-Location of the downdip end of seismic coupling and the continental shelf break. Journal of Geophysical Research: Solid Earth 126 (1). https://doi.org/10.1029/2020JB019589.

Malatesta, L.C., Finnegan, N.J., Huppert, K.L., Carreño, E.I., 2022. The influence of rock uplift rate on the formation and preservation of individual marine terraces during multiple sea-level stands. Geology 50 (1), 101–105. https://doi.org/10.1130/G49245.1.

Malinverno, A., 2012. Evolution of the Tyrrhenian Sea-Calabrian Arc system: The past and the present. In: Rendiconti Online della Società Geologica Italiana, 21, pp. 11–15.

Malinverno, A., Ryan, W.B.F., 1986. Extension in the Tyrrhenian Sea and shortening in the Apennines as a result of arc migration driven by sinking of the lithosphere. Tectonics 5, 227–245.

Matsu'ura, T., Komatsubara, J., Wu, C., 2019. Accurate determination of the Pleistocene uplift rate of the NE Japan forearc from the buried MIS 5e marine terrace shoreline angle. Quaternary Science Reviews 212, 45–68. https://doi.org/10.1016/j.quascirev.2019.03.007.

Melnick, D., 2016. Rise of the central Andean coast by earthquakes straddling the Moho. Nat. Geosci. 9 (5), 401–407. https://doi.org/10.1038/ngeo2683.

Merritts, D., Bull, W.B., 1989. Interpreting Quaternary uplift rates at the Mendocino triple junction, northern California, from uplifted marine terraces. Geology 17, 1020–1024.

Meschis, M., Roberts, G.P., Robertson, J., Briant, R.M., 2018. The relationships between regional Quaternary uplift, deformation across active normal faults, and historical seismicity in the upper plate of subduction zones: the Capo D'Orlando Fault, NE Sicily. Tectonics 37. https://doi.org/10.1029/2017TC004705.

Meschis, M., Roberts, G.P., Mildon, Z.K., Robertson, J., Michetti, A.M., Faure Walker, J. P., 2019. Slip on a mapped normal fault for the 28th December 1908 Messina earthquake (mw 7.1) in Italy. Scientific Reports 9 (1), 6481. https://doi.org/10.1038/s4159 8-019-42915-2.

Meschis, M., Roberts, G.P., Robertson, J., Mildon, Z.K., Sahy, D., Goswami, R., Sgambato, C., Faure Walker, J., Michetti, A.M., Iezzi, F., 2022. Out of phase Quaternary uplift-rate changes reveal normal fault interaction, implied by deformed marine palaeoshorelines. Geomorphology 416, 108432. https://doi.org/10.1016/j.geomorph.2022.108432.

Monaco, C., Tortorici, L., 2000. Active faulting in the Calabrian arc and eastern Sicily. J. Geodyn. 29, 407–424.

Monaco, C., Petronio, L., Romanelli, M., 1995. Tettonica estensionale nel settore orientale del Monte Etna (Sicilia): DATI morfotettonici e sismici. In: Proceedings of the Atti del Convegno Geodinamica e Tettonica Attiva del Sistema Tirreno-Appennino, Camerino, Italy, 9–10 February, pp. 363–374.

Monaco, C., Bianca, M., Catalano, S., De Guidi, G., Tortorici, L., 2002. Sudden change in the Late Quaternary tectonic regime in eastern Sicily: evidences from geological and geomorphological features. Boll. Soc. Geol. It. 901–913. Volume speciale n.1.

Monaco, C., Catalano, S., Cocina, O., De Guidi, G., Ferlito, C., Gresta, S., Musumeci, C., Tortorici, L., 2005. Tectonic control on the eruptive dynamics at Mt. Etna volcano (eastern Sicily) during the 2001 and 2002–2003 eruptions. J. Volcanol. Geotherm. Res. 144, 221–233.

Montgomery, D.R., Foufoula-Georgiou, E., 1993. Channel network source representation using digital elevation models. Water Resource Research 29, 3925–3934. https://doi.org/10.1029/93WR02463.

Nalin, R., Massari, F., Zecchin, M., 2007. Superimposed cycles of composite marine terraces: the example of Cutro terrace (Calabria, Southern Italy). J. Sediment. Res. 77 (4), 340–354. https://doi.org/10.2110/jsr.2007.030.

Nicol, A., Walsh, J.J., Villamor, P., Seebeck, K., Berryman, K.R., 2010. Normal fault interactions, paleoearthquakes and growth in an active rift. Journal of Structural Geology 32, 1101e1113.

Oakley, D.O., Kaufman, D.S., Gardner, T.W., Fisher, D.M., VanderLeest, R.A., 2017. Quaternary marine terrace chronology, North Canterbury, New Zealand, using amino acid racemization and infrared-stimulated luminescence. Quatern. Res. 87 (1), 151–167. https://doi.org/10.1017/qua.2016.9.

Olivetti, V., Balestrieri, M.L., Faccenna, C., Stuart, F.M., Vignaroli, G., 2010. Middle Miocene out-of-sequence thrusting and successive exhumation in the Peloritani Mountains, Sicily: late stage evolution of an orogen unraveled by apatite fission track and (U-Th)/He thermochronometry. Tectonics 29, TC5005. https://doi.org/10.1029/2009TC002659.

Olivetti, V., Cyr, A.J., Molin, P., Faccenna, C., Granger, D.E., 2012. Uplift history of the Sila Massif, southern Italy, deciphered from cosmogenic ^{10}Be erosion rates and river longitudinal profile analysis. Tectonics 31, 3. https://doi.org/10.1029/2011TC003037.

Pavano, F., 2013. Late Quaternary deformation of NE Sicily from relief and drainage system analysis. Rend. Online Soc. Geol. Ital. 29, 134–137.
Pavano, F., Gallen, S.F., 2021. A geomorphic examination of the Calabrian Forearc translation. Tectonics 40, e2020TC006692. https://doi.org/10.1029/2020TC006692.
Pavano, F., Catalano, S., Romagnoli, G., Tortorici, G., 2012. Dynamics and seismotectonics of NE Sicily. Rend. Online Soc. Geol. Ital. 21 (PART 1), 241–243.
Pavano, F., Romagnoli, G., Tortorici, G., Catalano, S., 2015. Active tectonics along the Nebrodi–Peloritani boundary in northeastern Sicily (southern Italy). Tectonophysics 659, 1–11. https://doi.org/10.1016/j.tecto.2015.07.024.
Pavano, F., Pazzaglia, F.J., Catalano, S., 2016. Knickpoints as geomorphic markers of active tectonics: a case study from northeastern Sicily (southern Italy). Lithosphere 8 (6), 633–648. https://doi.org/10.1130/L577.1.
Pavano, F., Catalano, S., Romagnoli, G., Tortorici, G., 2018. Hypsometry and relief analysis of the southern termination of the Calabrian arc, NE-Sicily (southern Italy). Geomorphology 304, 74–88.
Pavano, F., Pazzaglia, F.J., Rittenour, T.M., Catalano, S., Corbett, L.B., Bierman, P., 2024. Integrated uplift, subsidence, erosion and deposition in a tightly coupled source-to-sink system, Pagliara basin, northeastern Sicily, Italy. Basin Research 36, e12845. https://doi.org/10.1111/bre.12845.
Pazzaglia, F.J., Fisher, J., 2022. A reconstruction of Apennine uplift history and the development of transverse drainages from longitudinal profile inversion. In: Koeberl, C., Claeys, P., Montanari, S. (Eds.), From the Guajira Desert to the Apennines, and From Mediterranean Microplates to the Mexican Killer Asteroid, Geological Society of America Special Papers, p. 557.
Perron, J.T., Royden, L.H., 2013. An integral approach to bedrock river profile analysis. Earth Surf. Process. Landf. 38, 570–576. https://doi.org/10.1002/esp.3302.
Racano, S., Jara-Muñoz, J., Cosentino, D., Melnick, D., 2020. Variable quaternary uplift along the southern margin of the central Anatolian plateau inferred from modeling marine terrace sequences. Tectonics 39, e2019TC005921. https://doi.org/10.1029/2019TC005921.
Racano, S., Schildgen, T., Ballato, P., Yildirim, C., Wittmann, H., 2023. Rock-uplift history of the Central Pontides from river-profile inversions and implications for development of the North Anatolian Fault. Earth Planet. Sci. Lett. 616, 118231. https://doi.org/10.1016/j.epsl.2023.118231.
Racano, S., van der Beek, P.A., Schildgen, T.F., Faccenna, C., Buleo Tebar, V., Cosentino, D., 2024. Slab driven Quaternary rock-uplift and topographic evolution in the northern-central Apennines from linear inversion of the drainage system. Geochem. Geophys. Geosyst. 25, e2024GC011592. https://doi.org/10.1029/2024GC011592.
Roberts, G.P., Houghton, S.L., Underwood, C., Papanikolaou, I., Cowie, P.A., van Calsteren, P., Wigley, T., Cooper, F.J., McArthur, J.M., 2009. Localization of Quaternary slip rates in an active rift in 105 years: an example from central Greece constrained by 234U-230Th coral dates from uplifted paleoshorelines. J. Geophys. Res. 114, B10406. https://doi.org/10.1029/2008JB005818.
Roberts, G.P., Meschis, M., Houghton, S., Underwood, C., Briant, R.M., 2013. The implication of revised Quaternary paleoshoreline chronologies for the rates of active extension and uplift in the upper plate of subduction zone. Quaternary Sci. Rev. 78, 169–187. https://doi.org/10.1016/j.quascirev.2013.08.006.
Rohling, E.J., Foster, G.L., Grant, K.M., Marino, G., Roberts, A.P., Tamisiea, M.E., Williams, F., 2014. Sea-level and deep-sea-temperature variability over the past 5.3 million years. Nature 508 (7497), 477–482. https://doi.org/10.1038/nature13230.
Rosenbaum, G., Lister, G.S., 2004. Neogene and Quaternary rollback evolution of the Tyrrhenian Sea, the Apennines, and the Sicilian Maghrebides. Tectonics 23, TC1013. https://doi.org/10.1029/2003TC001518.
Rovida, A., Locati, M., Camassi, R., Lolli, B., Gasperini, P., Antonucci, A., 2022. Catalogo Parametrico dei Terremoti Italiani (CPTI15), versione 4.0. Istituto Nazionale di Geofisica e Vulcanologia (INGV). https://doi.org/10.13127/CPTI/CPTI15.4.
Rust, D., Kershaw, S., 2000. Holocene tectonic uplift patterns in northeastern Sicily: evidence from marine notches in coastal outcrops. Mar. Geol. 167, 105–126.
Saillard, M., Hall, S.R., Audin, L., Farber, D.L., Regard, V., Hérail, G., 2011. Andean coastal uplift and active tectonics in southern Peru: ^{10}Be surface exposure dating of differentially uplifted marine terrace sequences (San Juan de Marcona, 15.4°S). Geomorphology 128 (3–4), 178–190. https://doi.org/10.1016/j.geomorph.2011.01.004.
Scandone, P., 1979. Origin of the Tyrrhenian Sea and Calabrian Arc: Bollettino della Società Geologica Italiana, 98, pp. 27–34.
Scarfi', L., Barberi, G., Barreca, G., Cannavo', F., Koulakov, I., Patane', D., 2018. Slab narrowing in the Central Mediterranean: the Calabro-Ionian subduction zone as imaged by high resolution seismic tomography. Sci. Rep. 8, 5178. https://doi.org/10.1038/s41598-018-23543-8.
Scholz, C.H., Gupta, A., 2000. Fault interactions and seismic hazard. J. Geodyn. 29, 459–467.
Schwanghart, W., Scherler, D., 2014. Short Communication: TopoToolbox 2—MATLAB-based software for topographic analysis and modelling in Earth surface sciences. Earth Surf. Dyn. 2, 1–7. https://doi.org/10.5194/esurf-2-1-2014.
Schwanghart, W., Scherler, D., 2017. Bumps in river profiles: uncertainty assessment and smoothing using quantile regression techniques. Earth Surf. Dyn. 5, 821–839. https://doi.org/10.5194/esurf-5-821-2017.
Selli, R., 1978. Geologia e sismotettonica dello Stretto di Messina. Convegno: "L'attraversamento dello Stretto di Messina e la sua fattibilità", 4–6 Luglio 1978. Atti della Accademia Nazionale dei Lincei 43, 119–154.
Smith, A.G.G., Fox, M., Schwanghart, W., Carter, A., 2022. Comparing methods for calculating channel steepness index. Earth Sci. Rev. 227, 103970. https://doi.org/10.1016/j.earscirev.2022.103970.
Snyder, N.P., Whipple, K.X., Tucker, G.E., Merritts, D.J., 2000. Landscape response to tectonic forcing: Digital elevation model analysis of stream profiles in the Mendocino triple junction region, northern California. Geol. Soc. Am. Bull. 112 (8), 1250–1263.
Soliva, R., Benedicto, A., 2004. A linkage criterion for segmented normal faults. Journal of Structural Geology 12, 2251–2267.
Soliva, R., Benedicto, A., Maerten, L., 2006. Spacing and linkage of confined faults: the importance of mechanical thickness. J. Geophys. Res. 111, B01402. https://doi.org/10.1029/2004JB003507.
Soliva, R., Benedicto, A., Schultz, R.A., Maerten, L., Micarelli, L., 2008. Displacement and interaction of normal fault segments branched at depth: Implications for fault growth and potential earthquake rupture size. J. Struct. Geol. 30, 1288–1299.
Spampinato, C., Scicchitano, G., Ferranti, L., Monaco, C., 2012. Raised Holocene paleo-shorelines along the Capo Schisò coast, Taormina: New evidence of recent co-seismic deformation in northeastern Sicily (Italy). J. Geodyn. 55, 18–31. https://doi.org/10.1016/j.jog.2011.11.007.
Stewart, I., Cundy, A., Kershaw, S., Firth, C., 1997. Holocene coastal uplift in the Taormina area, northeastern Sicily: implications for the southern prolongation of the Calabrian seismogenic belt. J. Geodyn. 24, 37–50.
Totaro, C., Orecchio, B., Presti, D., Scolaro, S., Neri, G., 2016. Seismogenic stress field estimation in the Calabrian Arc region (south Italy) from a Bayesian approach. Geophys. Res. Lett. 43, 8960–8969. https://doi.org/10.1002/2016GL070107.
Trenhaile, A.S., 2019. Hard-rock coastal modelling: past practice and future prospects in a changing world. Journal of Marine Science and Engineering 7 (2), 34. https://doi.org/10.3390/jmse7020034.
Waelbroeck, C., Labeyrie, L., Michel, E., Duplessy, J.C., McManus, J.F., Lambeck, K., Balbon, E., Labracherie, M., 2002. Sea-level and deep water temperature changes derived from benthic foraminifera isotopic records. Quaternary Science Reviews 21, 295–305.
Weber, G.E., 1990. Late Pleistocene slip rates on the san Gregorio fault zone at point Año Nuevo, San Mateo County, California, stratigraphy and paleoceanographic history of the Monterey formation at Pt. Reyes and Pt. Año Nuevo, California. In: Pacific Section of the American Association of Petroleum Geologists Guidebook, 67, pp. 193–203.
Whipple, K.X., 2004. Bedrock rivers and the geomorphology of active orogens. Annu. Rev. Earth Planet. Sci. 32, 151–185. https://doi.org/10.1146/annurev.earth.32.101802.120356.
Whipple, K.X., Tucker, G.E., 1999. Dynamics of the stream power river incision model: Implications for height limits of mountain ranges, landscape response timescales and research needs. J. Geophys. Res. 104, 17,661–17,674. https://doi.org/10.1029/1999JB900120.
Whipple, K.X., Hancock, G.S., Anderson, R.S., 2000. River incision into bedrock: Mechanics and relative efficacy of plucking, abrasion, and cavitation. Geological Society of America Bulletin 112, 490–503. https://doi.org/10.1130/0016-7606(2000)12<490:RIIBMA>2.0.CO;2.
Willett, S.D., McCoy, S.W., Perron, J.T., Goren, L., Chen, C.-Y., 2014. Dynamic reorganization of river basins. Science 343, 1248765. https://doi.org/10.1126/science.1248765.
Wobus, C., Whipple, X.K., Kirby, E., Snyder, N., Johnson, J., Spyropolou, K., Crosby, B., Sheehan, D., 2006. Tectonics from topography: procedures, promise, and pitfalls. In: Willet, S.D., Hovius, N., Brandon, M.T., Fisher, D.M. (Eds.), Tectonics, Climate, and Landscape Evolution: Geologica Society of America Special Paper, Penrose Conference Series, 398, pp. 55–74. https://doi.org/10.1130/2006.2398(04.
Yildirim, C., Melnick, D., Ballato, P., Schildgen, T.F., Echtler, H., Erginal, A.E., Günec Kiyak, N., Strecker, M.R., 2013. Differential uplift along the northern margin of the central Anatolian plateau: inferences from marine terraces. Quat. Sci. Rev. 81, 12–28. https://doi.org/10.1016/j.quascirev.2013.09.011.